JOURNAL OF GEOPHYSICAL RESEARCH, VOL. 86, NO. C8, PAGES 7343-7362, AUGUST 20, 1981

Stratospheric Chemical and Thermal Response to Long-Term Variability in Solar UV Irradiance

G. BRASSEUR[1] AND P. C. SIMON

Institut d'Aéronomie Spatiale, 1180 Brussels, Belgium

A theoretical analysis of the chemical response of the stratosphere to possible long-term variability of solar ultraviolet irradiance has been performed, taking into account the thermal feedback effect on the reaction rates. Numerical values of ultraviolet and visible irradiation fluxes used in this work are given for aeronomic modeling purposes and a possible variability related to the 11-year solar cycle is suggested on the basis of recent and reliable observations of solar ultraviolet irradiance. This variability has been introduced in a stratospheric two-dimensional model which simulates the zonally averaged distribution of the chemical species related to the oxygen, hydrogen, nitrogen and chlorine families. The results lead to a total ozone variation of the order of 3% from the minimum to the maximum solar activity, with a maximum of about 10% in the upper stratosphere. At these heights, the calculated temperature change is close to 2–4 degrees. The N_2O concentration appears to be one of the most sensitive to long-term solar variability and a monitoring of this constituent would be useful to give information on the solar variability in the ultraviolet.

1. INTRODUCTION

Studies of the correlation between solar activity and the ozone concentration have a long history. The possibility of such a correlation which was first suggested by *Humphreys* [1910] has led to much controversy but numerous investigators [*Willett*, 1962; *London and Oltmans*, 1973; *Paetzold*, 1973; *Ruderman and Chamberlain*, 1975; *Angell and Korshover*, 1973, 1976], studying the statistics of the ozone data, have quoted a possible relationship between the content of this constituent and the sunspot number. However the observations are controversial because of absolute and intercalibration errors and gaps in data acquisition.

The effects of solar flux variabilities on atmospheric minor constituents have been prior to this work estimated by means of one-dimensional models. *Frederick* [1977] and *Rycroft and Theobald* [1978] have studied the chemical response of the upper stratosphere and mesosphere to variations of the solar irradiance with the 27-day solar rotation period. In particular, *Frederick* [1977] has determined the possible variation in the concentration of mesospheric ozone due to changes in the Lyman α line intensity. *Callis and Nealy* [1978*a*, *b*], *Penner and Chang* [1978] and *Callis et al.* [1979] have estimated the chemical and thermal response of the stratosphere to UV variability associated with the 11-year sunspot cycle adopting various possible solar flux variations among which some are close to irradiance ratio suggested by *Heath and Thekaekara* [1977]. Very recently, *Pollack et al.* [1979] have investigated the possible climatic impact of UV variations for time scales encompassing the 27-day solar rotation period, the sunspot period, the solar magnetic period and much longer times.

The purpose of this paper is to propose numerical values of UV and visible solar irradiance fluxes in a form which is convenient for aeronomic modeling purposes. The possible long-term variability of these fluxes will be discussed and a tentative amplitude of these changes versus wavelength will be proposed. The effect of such variability on the chemical and thermal structure of the stratosphere will be examined using a two-dimensional numerical model. In particular, the possible changes in the photodissociation rates of the atmospheric molecules will be studied and the modification of the rate constants due to the temperature variations will be taken into account. Only the flux variability associated with the 11-year cycle will be considered since the change of the solar flux intensity related to the 27-day solar rotation is less than 10% above 175 nm [*Heath*, 1973; *Hinteregger et al.*, 1977] and is of the same order of magnitude as the semi-annual variation in the solar constant (±3.3%) associated with the variation in the Sun-Earth distance.

2. THE SOLAR IRRADIATION FLUX AND ITS LONG-TERM VARIABILITY

Recently, *Simon* [1978, 1980] published a critical review of the available full disk measurements obtained during the solar cycle 20, between 120 and 400 nm, pointing out the disagreements between the most recent data. Since that time, new measurements have been made by *Heath* [1980], *Hinteregger* [1980], *Mount et al.* [1980] and *Simon et al.* [1981]. Table 1 gives the most useful observations for aeronomic purposes including date, accuracy and wavelength intervals. In fact, discrepancies of the order of 50% still exist for many data, especially in wavelengths particularly important for the photodissociation of molecular oxygen. Consequently, when dealing with atmospheric modeling, a critical study is necessary for the choice of the best solar irradiation flux values.

In the lower thermosphere, molecular oxygen is photodissociated by solar irradiation flux ranging from 130 to 175 nm, corresponding to the Schumann-Runge continuum. Only the data of *Rottman* [1981] *Mount et al.* [1980], *Hinteregger* [1980] and *Heroux and Swirbalus* [1976] cover this entire wavelength range, while values of *Samain and Simon* [1976] and *Kjeldseth Moe et al.* [1976] begin at 150 and 140 nm, respectively. They are not direct full disk irradiance measurements but they were determined from radiance measurements converted into mean intensities using the center-to-limb variation measured by *Samain and Simon* [1976]. The main objective of the observations of *Hinteregger* [1980] made from the AE-E satellite is to determine the variation of the solar irradiance from 14 to 185 nm. The absolute values are referring to the solar irradiance measurements of April 23, 1974, obtained by means of a

[1] Aspirant au Fonds National de la Recherche Scientifique.

Paper number 1C0139.
0148-0227/81/001C-0139$01.00

TABLE 1. Observational Data

Reference	Date of Observation	Wavelength Interval, nm	Vehicle	Accuracy, %
Arvensen et al. [1969]	Aug.–Nov. 1967	300–2500	aircraft	±25 to ±3
Broadfoot [1972]	June 15, 1970	210–320	rocket	±10
Simon [1974, 1975]	Sept. 23, 1972	196–230	balloon	±20
	May 16, 1973	285–355		±10
Rottman [1981]	Dec. 13, 1972	116–185	rocket	±15
	Aug. 30, 1973			
Samain and Simon [1976]	April 17, 1973	151–209	rocket	±30
Brueckner et al. [1976]	Sept. 4, 1973	174–210	rocket	±20
Heroux and Swirbalus [1976]	Nov. 2, 1973	123–194	rocket	±20
Heroux and Hinteregger [1978]	April 23, 1974	25–194	rocket	±20
Simon et al. [1981]	July 1, 1976	210–240	balloon	±15
	July 7, 1977	275–330		±10
Heath [1980]	Nov. 7, 1978	160–400	satellite	±10 to ±3
Hinteregger [1980]	July 1976 to Jan. 22, 1979	15–185	satellite	±20

rocket experiment [*Heroux and Hinteregger*, 1978]. For these reasons, the rocket measurements performed by *Rottman* [1981], by *Heroux and Swirbalus* [1976] and by *Mount et al.* [1980] seem to us to be the most reliable observations for aeronomic purposes between 120 and 175 nm. We have chosen Rottman's data obtained on December 13, 1972, to elaborate solar irradiance values averaged over 500 cm^{-1} because this observation took place in the middle of the second part of solar cycle 20, and not the value of *Mount et al.* [1980] which correspond to a maximum of solar activity during the solar cycle 21. A more complete discussion on these data is given by *Simon* [1981].

Below 90 km, photodissociation of molecular oxygen is due to solar radiation ranging from 175 to 240 nm. This process initiates the photochemistry in the mesosphere and in the upper stratosphere. Unfortunately, large discrepancies also exist in the wavelength range mainly between 180 and 190 nm (cf. Figure 6 of *Simon* [1978]) although rather good agreement exists at 175 nm between *Heroux and Swirbalus* [1976], *Brueckner et al.* [1976] and *Samain and Simon* [1976]. Therefore it seems appropriate to use between 175 and 200 nm the measurements of *Samain and Simon* [1976] in order to link Rottman's data with the values of *Simon* [1974] around 200 nm which have been confirmed by the new observations of *Heath* [1980]. Beyond 210 nm, these latter measurements are lower by a factor varying between 7 and 13% than the previous values of *Simon* [1974] but 27% higher than the recent values obtained by *Mount et al.* [1980] up to 255 nm. A complete discussion on the discrepancies between all these data has been presented by *Simon* [1981]. Consequently, the values of *Broadfoot* [1972], generally adopted for aeronomic purposes for the wavelengths beyond 230, would be adjusted taking into account the new measurements of *Heath* [1980], *Mount et al.* [1980] and *Simon et al.* [1981]. Nevertheless, the lowest data of Mount need to be confirm especially by new rocket observations including solar measurements beyond 255 nm because at longer wavelengths, around 290 nm, both *Simon* [1975] and *Heath* [1980] are in very good agreement with *Broadfoot* [1972].

According to the discussion already published by *Simon* [1978] on the irradiance data available beyond 290 nm, irradiation flux values obtained by balloon by *Simon* [1975] have been adopted up to 330 nm. These values are, in addition, in good agreement with the satellite measurement of *Heath* [1980] and the new balloon observation of *Simon et al.* [1981]. The data of *Arvesen et al.* [1969] were generally used from 330 nm up to near infrared. Unfortunately, the absolute scale used for calibration suffers from uncertainties [*Kostkowski*, 1974] and it seems preferable to consider the data of *Arvesen et al.* [1969] as a good relative spectral distribution at medium resolution. The latter values have to be adjusted to the data of *Neckel and Labs* [1981].

Tables 2 and 3 give the solar irradiation flux proposed for aeronomical calculations. The values correspond by definition to a mean solar activity and are averaged over several spectral intervals depending on the wavelength range.

As long-term variability of UV solar irradiance is quite evident at Lyman α and below 100 nm [*Vidal-Madjar*, 1975; *Schmidtke*, 1978], such a variation is expected at longer wavelength with a magnitude which has to be established. Unfortunately, in the wavelength range of stratospheric interest, the evidence of variations during solar cycle 20 is not conclusive as it was stated by *Simon* [1978] and by *Delaboudinière et al.* [1978]. This is due to the inadequate time coverage of reliable data during the solar cycle 20, to the uncertainties associated with each observation and to the absence of intercomparison in the calibration procedures. Nevertheless, *Heath and Thekaekara* [1977] claimed an 11-year variability of a factor of 2 at 200 nm on the basis of their own measurements performed by satellites and by rockets since 1966. This is illustrated in Figure 1 on which the full squares and triangles represent the solar flux ratio from minimum to maximum solar activity obtained from broadband photometric observations and the full circles the ratio obtained by means of a double monochromator experiment. The solid curve represents the solar variability deduced by the authors. It should be pointed out that there are only two points around 180 nm and that the solar flux ratios obtained around 290 nm with the double monochromator are 15–20% higher than those obtained from the broadband detectors at the same wavelength. In addition, the accuracy of the basic measurements obtained from this latter instrument is ±15% and ±30% for the shorter and the longer wavelength, respectively, and between ±8% and ±3% for the double monochromator data. A linear regression calculation is shown by the dashed lines for each set of solar flux ratios. Extrapolation of solar flux ratio at 340 nm from the broadband detector measurements gives a variability of 25% between irradiances corresponding to the maximum and to the minimum of the 11-year solar cycle. Such a value is in contradiction with the variability based on the double mono-

TABLE 2. Solar Irradiation Flux q at 1 AU

Number	$\Delta\lambda$, nm	$\Delta\nu$, cm^{-1}	q, $h\nu\ s^{-1}\ cm^{-2}$
	Averaged Over 500 cm^{-1} Between 117 and 308 nm		
1	Ly α 121.567	82,259	3.0×10^{11}
2	116.3–117.0	85,500–86,000	8.53×10^{8}
3	117.0–117.6	85,000–85,500	3.46×10^{9}
4	117.6–118.3	84,500–85,000	9.05×10^{8}
5	118.3–119.0	84,000–84,500	8.07×10^{8}
6	119.0–119.8	83,500–84,000	1.93×10^{9}
7	119.8–120.5	83,000–83,500	1.74×10^{9}
8	120.5–121.2	82,500–83,000	7.11×10^{9}
9	121.2–122.0	82,000–82,500	3.25×10^{11}
10	122.0–122.7	81,500–82,000	2.60×10^{9}
11	122.7–123.5	81,000–81,500	1.43×10^{9}
12	123.5–124.2	80,500–81,000	1.23×10^{9}
13	124.2–125.0	80,000–80,500	1.23×10^{9}
14	125.0–125.8	79,500–80,000	7.34×10^{8}
15	125.8–126.6	79,000–79,500	2.17×10^{9}
16	126.6–127.4	78,500–79,000	6.80×10^{8}
17	127.4–128.2	78,000–78,500	1.02×10^{9}
18	128.2–129.0	77,500–78,000	7.23×10^{8}
19	129.0–129.9	77,000–77,500	8.37×10^{8}
20	129.9–130.7	76,500–77,000	5.89×10^{9}
21	130.7–131.6	76,000–76,500	4.65×10^{9}
22	131.6–132.4	75,500–76,000	9.74×10^{8}
23	132.4–133.3	75,000–75,500	1.01×10^{9}
24	133.3–134.2	74,500–75,000	8.92×10^{9}
25	134.2–135.1	74,000–74,500	1.01×10^{9}
26	135.1–136.0	73,500–c4,000	2.29×10^{9}
27	136.0–137.0	73,000–73,500	1.75×10^{9}
28	137.0–137.9	72,500–73,000	1.49×10^{9}
29	137.9–138.9	72,000–72,500	1.72×10^{9}
30	138.9–140.8	71,000–72,000	9.46×10^{9}
31	140.8–142.8	70,000–71,000	4.94×10^{9}
32	142.8–144.9	69,000–70,000	6.36×10^{9}
33	144.9–147.0	68,000–69,000	7.79×10^{9}
34	147.0–149.2	67,000–68,000	1.21×10^{10}
35	149.2–151.5	66,000–67,000	1.37×10^{10}
36	151.5–153.8	65,000–66,000	2.01×10^{10}
37	153.8–156.2	64,000–65,000	3.58×10^{10}
38	156.2–158.7	63,000–64,000	2.93×10^{10}
39	158.7–161.3	62,000–63,000	3.42×10^{10}
40	161.3–163.9	61,000–62,000	4.41×10^{10}
41	163.9–166.7	60,000–61,000	8.02×10^{10}
42	166.7–169.5	59,000–60,000	1.11×10^{11}
43	169.5–172.4	58,000–59,000	1.97×10^{11}
44	172.4–173.9	57,500–58,000	1.21×10^{10}
45	173.9–175.4	57,000–57,500	1.44×10^{11}
46	175.4–177.0	56,500–57,000	1.33×10^{11}
47	177.0–178.6	56,000–56,500	1.96×10^{11}
48	178.6–180.2	55,500–56,000	2.12×10^{11}
49	180.2–181.8	55,000–55,500	2.79×10^{11}
50	181.8–183.5	54,500–55,000	3.24×10^{11}
51	183.5–185.2	54,000–54,500	3.03×10^{11}
52	185.2–186.9	53,500–54,000	3.74×10^{11}
53	186.9–188.7	53,000–53,500	4.93×10^{11}
54	188.7–190.5	52,500–53,000	5.21×10^{11}
55	190.5–192.3	52,000–52,500	6.08×10^{11}
56	192.3–194.2	51,500–52,000	5.57×10^{11}
57	194.2–196.1	51,000–51,500	8.49×10^{11}
58	196.1–198.0	50,500–51,000	9.39×10^{11}
59	198.0–200.0	50,000–50,500	1.05×10^{12}
60	200.0–202.0	49,500–50,000	1.44×10^{12}
61	202.0–204.1	49,000–49,500	1.80×10^{12}
62	204.1–206.2	48,500–49,000	2.08×10^{12}
63	206.2–208.3	48,000–48,500	2.45×10^{12}
64	208.3–210.5	47,500–48,000	5.09×10^{12}
65	210.5–212.8	47,000–47,500	7.12×10^{12}
66	212.8–215.0	46,500–47,000	8.55×10^{12}
67	215.0–217.4	46,000–46,500	9.27×10^{12}
68	217.4–219.8	45,500–46,000	1.16×10^{13}
69	219.8–222.2	45,000–45,500	1.20×10^{13}
70	222.2–224.7	44,500–45,000	1.64×10^{13}
71	224.7–227.3	44,000–44,500	1.41×10^{13}
72	227.3–229.9	43,500–44,000	1.48×10^{13}
73	229.9–232.6	43,000–43,500	1.68×10^{13}
74	232.6–235.3	42,500–43,000	1.45×10^{13}
75	235.3–238.1	42,000–42,500	1.74×10^{13}
76	238.1–241.0	41,500–42,000	1.54×10^{13}
77	241.0–243.9	41,000–41,500	2.25×10^{13}
78	243.9–246.9	40,500–41,000	2.05×10^{13}
79	246.9–250.0	40,000–40,500	2.09×10^{13}
80	250.0–253.2	39,500–40,000	2.03×10^{13}
81	253.2–256.4	39,000–39,500	2.96×10^{13}
82	256.4–259.7	38,500–39,000	5.45×10^{13}
83	259.7–263.2	38,000–38,500	4.86×10^{13}
84	263.2–266.7	37,500–38,000	1.19×10^{14}
85	266.7–270.3	37,000–37,500	1.29×10^{14}
86	270.3–274.0	36,500–37,000	1.17×10^{14}
87	274.0–277.8	36,000–36,500	1.11×10^{14}
88	277.8–281.7	35,500–36,000	7.84×10^{13}
89	281.7–285.7	35,000–35,500	1.50×10^{14}
90	285.7–289.9	34,500–35,000	2.12×10^{14}
91	289.9–294.1	34,000–34,500	3.56×10^{14}
92	294.1–298.5	33,500–34,000	3.33×10^{14}
93	298.5–303.0	33,000–33,500	3.08×10^{14}
94	303.0–307.7	32,500–33,000	4.39×10^{14}
	Averaged Over 5 nm Between 307.5 and 647.5 nm		
95	307.5–312.5		4.91×10^{14}
96	312.5–317.5		5.53×10^{14}
97	317.5–322.5		6.04×10^{14}
98	322.5–327.5		6.97×10^{14}
99	327.5–332.5		8.49×10^{14}
100	332.5–337.5		7.52×10^{14}
101	337.5–342.5		8.13×10^{14}
102	342.5–347.5		7.84×10^{14}
103	347.5–352.5		8.31×10^{14}
104	352.5–357.5		9.33×10^{14}
105	357.5–362.5		8.47×10^{14}
106	362.5–367.5		1.06×10^{15}
107	367.5–372.5		1.10×10^{15}
108	372.5–377.5		9.57×10^{14}
109	377.5–382.5		1.14×10^{15}
110	382.5–387.5		8.63×10^{14}
111	387.5–392.5		1.15×10^{15}
112	392.5–397.5		9.57×10^{14}
113	397.5–402.5		1.70×10^{15}
114	402.5–407.5		1.70×10^{15}
115	407.5–412.5		1.78×10^{15}
116	412.5–417.5		1.87×10^{15}
117	417.5–422.5		1.84×10^{15}
118	422.5–427.5		1.80×10^{15}
119	427.5–432.5		1.66×10^{15}
120	432.5–437.5		2.04×10^{15}
121	437.5–442.5		2.00×10^{15}
122	442.5–447.5		2.20×10^{15}
123	447.5–452.5		2.35×10^{15}
124	452.5–457.5		2.30×10^{15}
125	457.5–462.5		2.35×10^{15}
126	462.5–467.5		2.34×10^{15}
127	467.5–472.5		2.36×10^{15}
128	472.5–477.5		2.39×10^{15}
129	477.5–482.5		2.49×10^{15}
130	482.5–487.5		2.30×10^{15}
131	487.5–492.5		2.36×10^{15}
132	492.5–497.5		2.53×10^{15}
133	497.5–502.5		2.38×10^{15}
134	502.5–507.5		2.47×10^{15}
135	507.5–512.5		2.47×10^{15}
136	512.5–517.5		2.32×10^{15}
137	517.5–522.5		2.46×10^{15}
138	522.5–527.5		2.43×10^{15}
139	527.5–532.5		2.60×10^{15}
140	532.5–537.5		2.59×10^{15}
141	537.5–542.5		2.51×10^{15}
142	542.5–547.5		2.56×10^{15}
143	547.5–552.5		2.61×10^{15}
144	552.5–557.5		2.57×10^{15}
145	557.5–562.5		2.55×10^{15}
146	562.5–567.5		2.61×10^{15}
147	567.5–572.5		2.63×10^{15}
148	572.5–577.5		2.68×10^{15}
149	577.5–582.5		2.66×10^{15}

TABLE 2. (continued)

Number	Δλ, nm	Δν, cm^{-1}	q, $h\nu\ s^{-1}\ cm^{-2}$
Averaged Over 5 nm Between 307.5 and 647.5 nm (continued)			
150	582.5–587.5		2.68×10^{15}
151	587.5–592.5		2.60×10^{15}
152	592.5–597.5		2.67×10^{15}
153	597.5–602.5		2.59×10^{15}
154	602.5–607.5		2.70×10^{15}
155	607.5–612.5		2.64×10^{15}
156	612.5–617.5		2.62×10^{15}
157	617.5–622.5		2.67×10^{15}
158	622.5–627.5		2.62×10^{15}
159	627.5–632.5		2.61×10^{15}
160	632.5–637.5		2.64×10^{15}
161	637.5–642.5		2.62×10^{15}
162	642.5–647.5		2.66×10^{15}
Averaged Over 10 nm Between 645 and 735 nm			
163	645–655		5.21×10^{15}
164	655–665		5.07×10^{15}
165	665–675		5.24×10^{15}
166	675–685		5.15×10^{15}
167	685–695		5.11×10^{15}
168	695–705		5.03×10^{15}
169	705–715		5.00×10^{15}
170	715–725		4.91×10^{15}
171	725–735		4.90×10^{15}

chromator data. On the other hand, extrapolation of the latter data to shorter wavelength gives a ratio of only 0.7 at 200 nm. If variations with the 11-year cycle in the ultraviolet solar irradiance do exist, they are probably less than those stated by *Heath and Thekaekara* [1977].

Such a comment seems to be confirmed by *Hinteregger* [1980] for observations performed between 1976 and 1979 for wavelengths below 185 nm, leading to a variability of 21% around 180 nm during that time and by new observations performed by balloon in 1976 and 1977 [*Simon et al.*, 1981] corresponding to the minimum solar activity between solar cycle 20 and 21. Variations between 210 and 240 nm over the 11-year cycle may not exceed 20% if differences between observations are interpreted only as variations of the solar output and not as experimental errors.

The previous considerations lead us to adopt a solar irradiance ratio between the minimum and the maximum of the 11-year cycle varying from 0.8 at 200 nm to 1 at 300 nm. These ratios are illustrated in Figure 2 and have been introduced in our calculations.

3. Theoretical Response of the Stratosphere to UV Variability Associated With the 11-Year Sunspot Cycle

Using a two-dimensional model of the stratosphere which has been described in several previous papers [*Brasseur*, 1976, 1978*a*, *b*; *Brasseur and Bertin*, 1977, 1978], we have studied the relationship between the solar variability and the stratospheric minor constituents at various latitudes. The model has been used with steady state conditions since the run of the time dependent version for a period of 2 or 3 solar cycles consumes a prohibitive amount of computer time. A thermal scheme has been added to the chemical approach in order to take into account the thermal feedback in the chemical responses. The distribution in the meridional plane of the following species is calculated: O_3, $O(^3P)$, $O(^1D)$, OH, HO_2, N_2O, NO, NO_2, N_2O_5, HNO_3, CH_4, CH_3Cl, $CFCl_3$, CF_2Cl_2, CCl_4, Cl, ClO, $ClONO_2$, HCl. The water vapor is being held con-

TABLE 3. Solar Irradiation Flux q at 1 AU Averaged Over 1 nm Between 120 and 310 nm

Δλ, nm	q, $h\nu\ s^{-1}\ cm^{-2}\ nm^{-1}$
120–121	6.30×10^{9}
121–122	3.06×10^{11}
122–123	3.40×10^{9}
123–124	1.58×10^{9}
124–125	1.50×10^{9}
125–126	1.14×10^{9}
126–127	2.10×10^{9}
127–128	1.17×10^{9}
128–129	9.50×10^{8}
129–130	9.68×10^{8}
130–131	8.38×10^{9}
131–132	1.73×10^{9}
132–133	1.17×10^{9}
133–134	9.88×10^{9}
134–135	1.07×10^{9}
135–136	2.38×10^{9}
136–137	1.75×10^{9}
137–138	1.67×10^{9}
138–139	1.71×10^{9}
139–140	5.21×10^{9}
140–141	4.12×10^{9}
141–142	2.40×10^{9}
142–143	2.68×10^{9}
143–144	3.09×10^{9}
144–145	3.13×10^{9}
145–146	3.23×10^{9}
146–147	4.19×10^{9}
147–148	5.24×10^{9}
148–149	5.70×10^{9}
149–150	5.34×10^{9}
150–151	6.19×10^{9}
151–152	6.43×10^{9}
152–153	8.77×10^{9}
153–154	9.49×10^{9}
154–155	1.74×10^{10}
155–156	1.42×10^{10}
156–157	1.37×10^{10}
157–158	1.17×10^{10}
158–159	1.16×10^{10}
159–160	1.23×10^{10}
160–161	1.35×10^{10}
161–162	1.50×10^{10}
162–163	1.78×10^{10}
163–164	2.01×10^{10}
164–165	2.40×10^{10}
165–166	3.52×10^{10}
166–167	2.97×10^{10}
167–168	3.29×10^{10}
168–169	4.21×10^{10}
169–170	5.75×10^{10}
170–171	6.83×10^{10}
171–172	7.02×10^{10}
172–173	7.68×10^{10}
173–174	7.81×10^{10}
174–175	9.26×10^{10}
175–176	7.40×10^{10}
176–177	8.50×10^{10}
177–178	1.15×10^{11}
178–179	1.32×10^{11}
179–180	1.29×10^{11}
180–181	1.54×10^{11}
181–182	2.00×10^{11}
182–183	1.86×10^{11}
183–184	1.97×10^{11}
184–185	1.66×10^{11}
185–186	1.91×10^{11}
186–187	2.37×10^{11}
187–188	2.66×10^{11}
188–189	2.80×10^{11}
189–190	2.93×10^{11}
190–191	2.94×10^{11}
191–192	3.33×10^{11}

TABLE 3. (continued)

Δλ, nm	q, $h\nu$ s^{-1} cm^{-2} nm^{-1}
192–193	3.48×10^{11}
193–194	2.54×10^{11}
194–195	4.46×10^{11}
195–196	4.27×10^{11}
196–197	4.86×10^{11}
197–198	4.87×10^{11}
198–199	4.92×10^{11}
199–200	5.53×10^{11}
200–201	7.11×10^{11}
201–202	7.29×10^{11}
202–203	8.04×10^{11}
203–204	8.93×10^{11}
204–205	9.76×10^{11}
205–206	9.90×10^{11}
206–207	1.06×10^{12}
207–208	1.20×10^{12}
208–209	1.53×10^{12}
209–210	2.56×10^{12}
210–211	2.92×10^{12}
211–212	3.61×10^{12}
212–213	3.23×10^{12}
213–214	3.43×10^{12}
214–215	4.43×10^{12}
215–216	4.01×10^{12}
216–217	3.73×10^{12}
217–218	3.96×10^{12}
218–219	4.95×10^{12}
219–220	5.27×10^{12}
220–221	5.35×10^{12}
221–222	4.39×10^{12}
222–223	5.68×10^{12}
223–224	7.42×10^{12}
224–225	6.55×10^{12}
225–226	6.13×10^{12}
226–227	4.68×10^{12}
227–228	4.69×10^{12}
228–229	6.22×10^{12}
229–230	5.53×10^{12}
230–231	6.54×10^{12}
231–232	5.83×10^{12}
232–233	6.43×10^{12}
233–234	5.40×10^{12}
234–235	4.65×10^{12}
235–236	6.76×10^{12}
236–237	5.87×10^{12}
237–238	6.38×10^{12}
238–239	5.04×10^{12}
239–240	5.61×10^{12}
240–241	5.22×10^{12}
241–242	6.39×10^{12}
242–243	8.86×10^{12}
243–244	8.03×10^{12}
244–245	7.69×10^{12}
245–246	6.33×10^{12}
246–247	6.40×10^{12}
247–248	7.13×10^{12}
248–249	5.66×10^{12}
249–250	7.35×10^{12}
250–251	7.48×10^{12}
251–252	5.91×10^{12}
252–253	5.60×10^{12}
253–254	7.09×10^{12}
254–255	7.80×10^{12}
255–256	1.14×10^{13}
256–257	1.38×10^{13}
257–258	1.68×10^{13}
258–259	1.75×10^{13}
259–260	1.41×10^{13}
260–261	1.34×10^{13}
261–262	1.36×10^{13}
262–263	1.60×10^{13}
263–264	2.33×10^{13}
264–265	3.65×10^{13}
265–266	3.75×10^{13}
266–267	3.50×10^{13}
267–268	3.64×10^{13}
268–269	3.52×10^{13}
269–270	3.43×10^{13}
270–271	4.00×10^{13}
271–272	3.18×10^{13}
272–273	2.95×10^{13}
273–274	2.81×10^{13}
274–275	1.90×10^{13}
275–276	2.78×10^{13}
276–277	3.60×10^{13}
277–278	3.36×10^{13}
278–279	2.33×10^{13}
279–280	1.26×10^{13}
280–281	1.59×10^{13}
281–282	3.28×10^{13}
282–283	4.37×10^{13}
283–284	4.71×10^{13}
284–285	3.50×10^{13}
285–286	2.03×10^{13}
286–287	4.62×10^{13}
287–288	5.38×10^{13}
288–289	4.46×10^{13}
289–290	6.65×10^{13}
290–291	9.12×10^{13}
291–292	8.82×10^{13}
292–293	8.04×10^{13}
293–294	8.07×10^{13}
294–295	7.56×10^{13}
295–296	8.17×10^{13}
296–297	7.36×10^{13}
297–298	7.97×10^{13}
298–299	6.21×10^{13}
299–300	7.32×10^{13}
300–301	6.10×10^{13}
301–302	6.77×10^{13}
302–303	7.38×10^{13}
303–304	9.65×10^{13}
304–305	9.37×10^{13}
305–306	8.93×10^{13}
306–307	8.89×10^{13}
307–308	1.00×10^{14}
308–309	9.54×10^{13}
309–310	7.55×10^{13}

stant; since H_2O appears to be less sensitive to the photochemistry than to the transport, this hypothesis should not seriously alter out conclusions.

The steady state assumption needs further justification since species with long chemical lifetime (N_2O, CH_4, $CFCl_3$, CF_2Cl_2, etc.) may be expected to respond with a certain delay

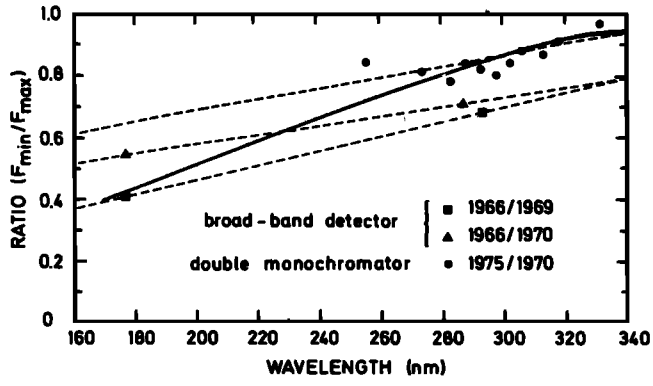

Fig. 1. Ratio of solar flux measured near solar cycle minimum to that measured near solar cycle maximum versus wavelength claimed by *Heath and Thekaekara* [1977] (solid line). The full squares and triangles are based on broadband photometric observations and the full circles on a double monochromator experiment.

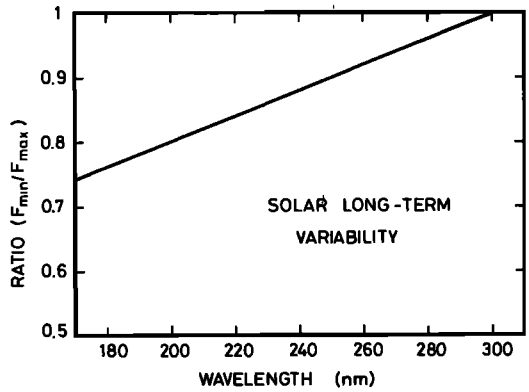

Fig. 2. Long-term solar variability adopted in this work. The curve representing the ratio between minimum and maximum irradiance refers to an upper limit of variability during the 11-year sunspot cycle.

which is not negligible compared with 11 years. In fact, the variability of minor constituents appears with the highest efficiency in the regions where the photochemistry is the most active, that is where the lifetime of the species is the shortest. As shown by *Callis and Nealy* [1978*a*, *b*] and by *Penner and Chang* [1978], in their 1-D models, the time lag for long lived species such as N_2O is significant only in the altitude range where the magnitude of the variation is very small. The calculated ozone change by these authors using a full interactive time dependent calculation, is thus nearly identical to that obtained with a steady state model.

On the other hand, there may be significant differences between steady and time-dependent calculations for more reactive species such as HNO_3, H_2O_2 and $ClONO_2$ leading in steady state models to errors in the calculations of both local and total ozone. Again, this effect and the possible significant phase difference with respect to solar activity appears essentially in the lower stratosphere where the relative ozone variation is the smallest. Nevertheless further investigation should estimate the impact of seasonal variations in the calculations, particularly in a two-dimensional representation.

In order to determine the concentration of constituents (or family of constituents such as NO_y (= NO + NO_2 + HNO_3 + $2N_2O_5$ + $ClONO_2$) or ClX (= Cl + ClO + HCl + $ClONO_2$)) we have solved for each of them a continuity equation. The meridional distribution of the temperature T is obtained by solving the equation of energy conservation.

A detailed description of the model with the related numerical method and the physical and chemical conditions is given in the appendix.

4. Analysis of the Results

The model has been run for three different scenarios. In the first case, a solar flux q_{mean} corresponding to average irradiance conditions is adopted; the second and third cases refer respectively to high (q_{max}) and low (q_{min}) solar activity. The fractional variation of a quantity X, expressed in percent, is then defined as

$$\frac{\Delta X}{X} = \frac{X(q_{max}) - X(q_{min})}{X(q_{mean})} \times 100$$

The temperature variation however is expressed by its absolute value

$$\Delta T = T(q_{max}) - T(q_{min})$$

The primary effect of the solar flux variation as shown by Figure 2 appears through a change in the photodissociation rates for the molecules absorbing below 300 nm. Figure 3 shows the relative variation of photodissociation frequencies for various stratospheric species. Due to larger variations of ultraviolet flux around 200 nm, compounds absorbing mainly in the shorter wavelengths range are obviously more sensitive than constituents whose absorption peaks are observed in the visible or in the near UV. For example, when the solar irradiance increases from the minimum to the maximum, the production rate of ozone related to the dissociation of O_2 increases more significantly than the dissociation of O_3.

The second chemical response appears through the change in the temperature distribution since chemical reaction rates are generally temperature dependent. This effect is not negligible as shown by the following example which refers to simplified conditions. If a pure oxygen atmosphere is assumed, the ozone concentration above 25–30 km is given by [*Nicolet*, 1971]

$$n(O_3) = [J\, n(M)\, n^2(O_2)\, K]^{1/2}$$

where $K = k_2/k_3$ (see Table 3) and where $J = J_{O_2}/J_{O_3}$ is the ratio of the O_2 and O_3 photodissociation rates. The fractional variation in the ozone concentration can be written, if the molecular oxygen and total concentrations are assumed to remain unchanged,

$$\frac{\Delta n(O_3)}{n(O_3)} \simeq \frac{1}{2}\frac{\Delta J}{J} + \frac{1}{2}\frac{\Delta K}{K}$$

The first term, which is the direct effect via the photodissociation rates, is positive (Figure 4) since $\Delta J_{O_2}/J_{O_2} > \Delta J_{O_3}/J_{O_3}$. The second term which represents the indirect effect via the temperature change is negative since $\Delta K/K \cong -2810\Delta T/T^2$. In fact, the temperature dependence of the recombination rate of O and O_3 (reaction k_3, see Table 3) reduces the variation of the ozone concentration as computed when the temperature feedback is omitted. In the real atmosphere, the problem is more complex since the interaction with other constituents (HO_x, NO_x, ClX, etc.) has to be taken into consideration and the full model calculation has to be performed. However, the

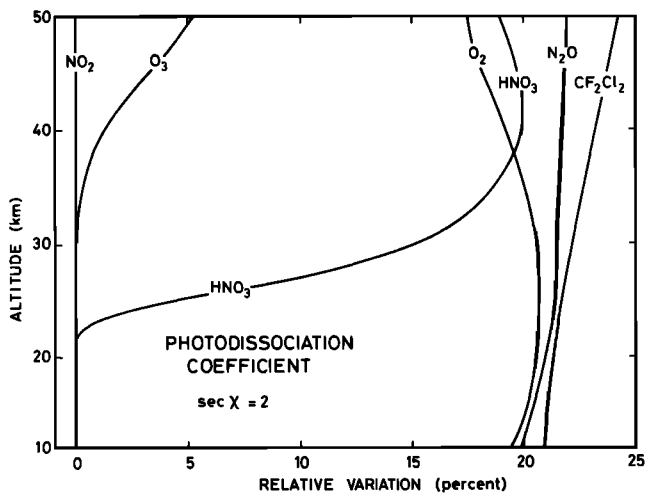

Fig. 3. Relative variation of the photodissociation frequency of various stratospheric species as a function of the altitude and for a solar zenith angle of 60 degrees.

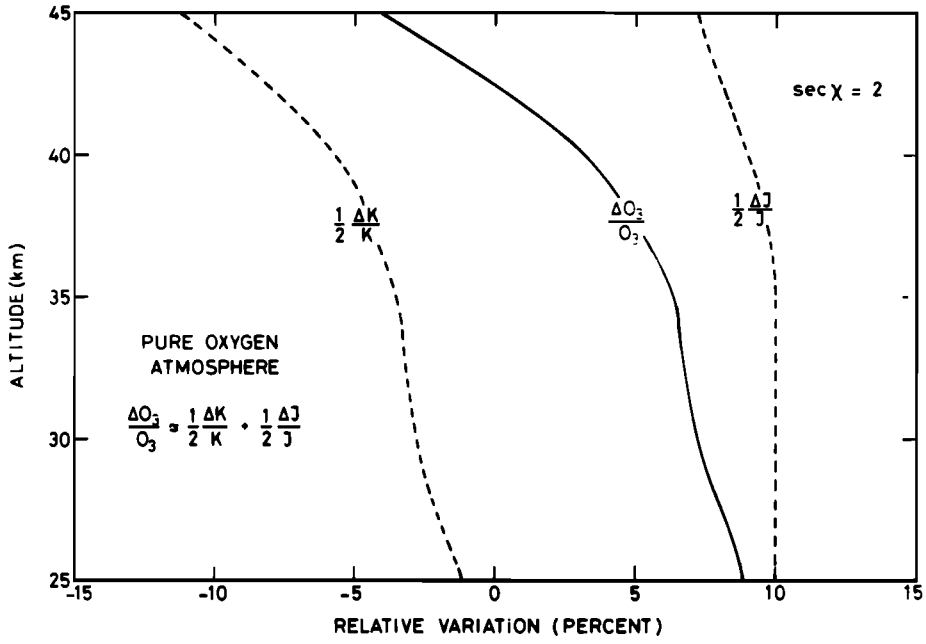

Fig. 4. Relative variation of the ozone concentration versus altitude in a pure oxygen atmosphere for a zenith angle of 60 degrees. The curve labelled $\Delta J/2J$ refers to the contribution of the change in the photodissociation rates while the curve labelled $\Delta K/2K$ represents the effect of the following temperature variations: $\Delta T = 0.4$ K at 25 km, 1.1 at 30 km, 1.6 at 35 km, 3.0 at 40 km, and 6.0 at 45 km.

temperature effect appears mainly through the direct recombination of O and O_3.

A third effect, which is not included in this work, could play a certain role, namely, the variation of the total concentration which, according to the hydrostatic law, should be associated with any temperature change. This variation could affect the three body reaction rates (see, for example, reactions k_2, a_1, etc., Table 4 in the appendix) and the concentration of minor constituents above 35–40 km [*Penner and Luther*, 1980].

Figure 5 depicts the percent change in ozone concentration from solar minimum to solar maximum, as computed in the 2-D model using the full chemistry of Table 4 (see appendix). Curve *a* represents the vertical distribution of O_3 at 30 degrees latitude when the temperature feedback is taken into account. In curve *b* the temperature is held constant. In this latter case, the ozone concentration increases with the solar flux, the maximum variation (13%) appearing around 40 km. This large increase of O_3 in the upper stratosphere is due to the enhanced dissociation rate of molecular oxygen in this altitude range. Moreover, in the vicinity of the stratopause (and in the lower mesosphere), the enhancement of O_3 becomes smaller due to the increase of the OH and HO_2 concentration. In the lower stratosphere, the increase of O_3 is relatively small since the penetration of UV radiation in the Herzberg continuum is reduced by the enhancement of the ozone content at higher alti-

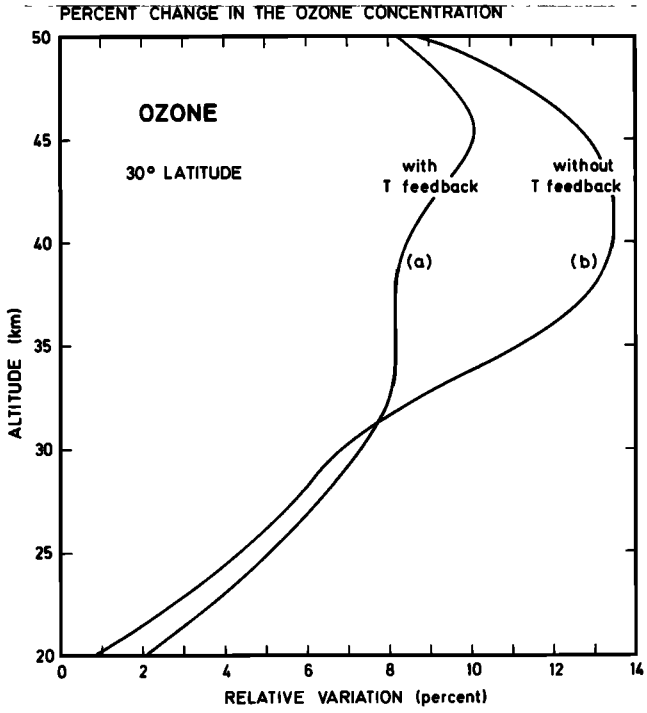

Fig. 5. Relative change of the ozone concentration versus altitude at 30 degrees latitude (yearly mean) related to the solar irradiance variation as indicated in Figure 2. Curve *a* with temperature feedback. Curve *b* with fixed temperature.

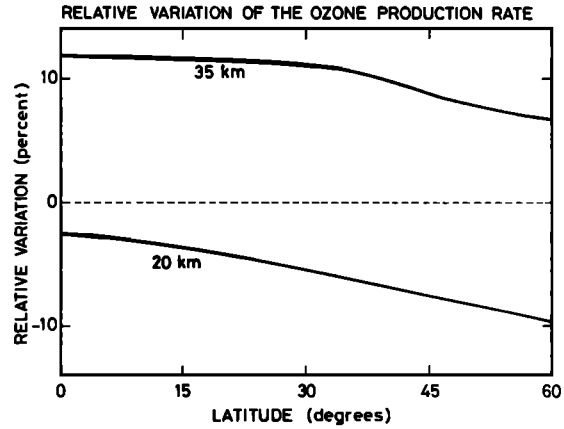

Fig. 6. Relative variation of the ozone production rate as a function of the latitude at 20 and 35 km, respectively.

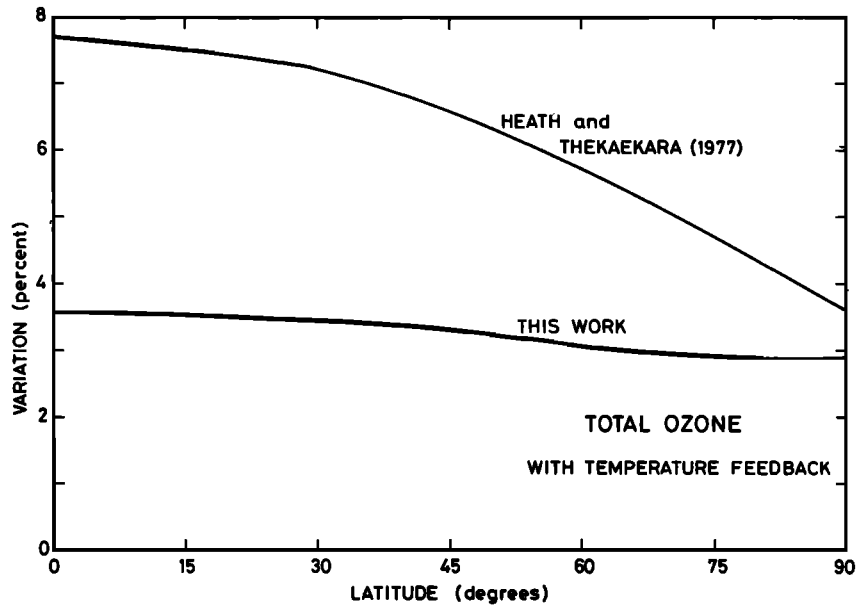

Fig. 7. Relative variation of the vertically integrated ozone concentration as a function of the latitude assuming two different solar flux variabilities (Figure 1—solid line—and Figure 2).

tude and by the fact that O_3 becomes less sensitive to chemistry and photochemistry. In order to illustrate this point, Figure 6 depicts the variation of the average ozone production rate at 35 and 20 km respectively. In the upper stratosphere of the equatorial regions, the photodissociation rate of O_2 leading to the formation of O_3 is increased by more than 10% from solar minimum to solar maximum. But in the lower stratosphere, due to the enhancement of the optical depth above this level, the production rate of ozone is reduced by a factor which increases with latitude (i.e., with optical depth or solar zenith angle). At 20 km this reduction varies from about 2% at the equator to 10% at 60 degrees latitude. The loss rate of O_3 is also modified. It increases with solar flux in the upper stratosphere so that a new photochemical equilibrium is reached with a corresponding value of the ozone concentration. In the lower stratosphere, the loss rate decreases with increasing solar irradiance but the new ozone concentration depends on the transport conditions which are kept unchanged in the present model.

When the temperature feedback is considered, the ozone variation as given by the model calculation, is reduced above 30 km and the maximum (10%) raises to about 45 km. This reduction is explained by the negative correlation between O_3 and temperature. Below 30 km, in the region where the peak of the ozone concentration is located, the ozone enhancement is slightly larger when the temperature feedback is considered. Again this is related to the variation of ozone at higher altitude and the penetration of UV radiation down to the lower stratosphere. With the spectral distribution of the solar variability adopted in this paper, the relative change of the ozone column has the same order of magnitude (3%) in both cases (with and without temperature feedback). Moreover, as stated by Figure 7, the total ozone variation $\Delta O_3/O_3$ does not show any appreciable latitudinal variation if the proposed solar variability is used in the model calculation. In fact, as shown in Figure 8, the equatorial regions are characterized by a relatively large ozone enhancement at high altitudes and a small variation at low altitudes, while at higher latitudes the ozone variation is relatively constant between 20 and 45 km. This effect can be explained by the feedback between the vertical ozone distribution and the penetration of the UV radiation responsible for the ozone formation.

Figure 9 shows, for comparison purposes, the ozone variations at 30° latitude due to the flux variability adopted in this work and those due to higher variability proposed by *Heath and Thekaekara* [1977]. The magnitude of the O_3 variation is enhanced from 10 to 22% at 45 km. Since this last number is much larger than the observed changes of the ozone concentration in the upper stratosphere [*Angell and Korshover, 1978a*], the solar flux variability given by *Heath and Thekaekara* [1977] is probably largely overestimated. When the latter

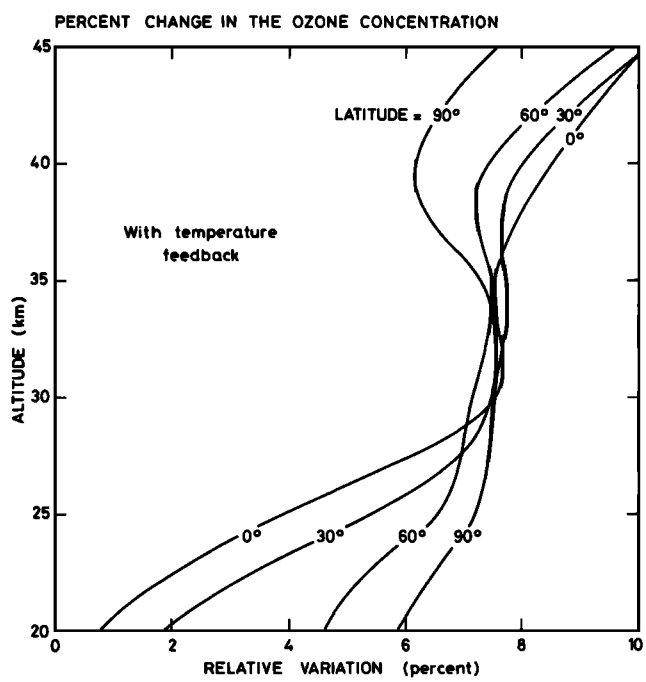

Fig. 8. Relative variation of the ozone concentration versus altitude at different latitudes in response to the UV variability from solar minimum to maximum (Figure 2).

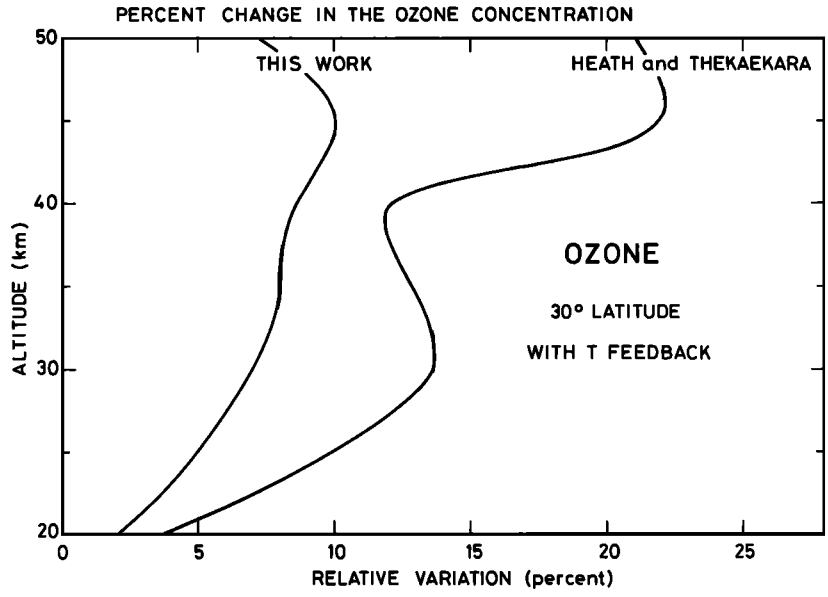

Fig. 9. Relative variation of the ozone concentration versus altitude for two different solar flux variabilities (see Figure 1—solid line—and Figure 2).

solar variability is introduced in the model calculation, the increase in the total ozone concentration shows a more pronounced latitudinal variation (Figure 7). This effect can be explained by the fact that, in this latter case, the solar irradiance is modified as far as 350 nm, i.e., in a region where ozone is photodissociated and molecular oxygen is not. Therefore, the variation of the J_O/J_O ratio is more sensitive to the solar zenith angle in the case of the Heath and Thekaekara model than in the case of the solar flux variability as suggested in this paper.

The numbers obtained in the present computation are not inconsistent with the analysis of the ozone data by *Angell and Korshover* [1978*a*]. These show in the northern hemisphere where most stations are located a 5% increase in total ozone between the early 1960's and 1970's and a 1–2% decrease between 1970 and 1972. The analysis of *Angell and Korshover* [1978*a*] also indicates that the Umkehr data in the north temperate latitudes suggest a 11% increase of the ozone concentration in the 32–46 km layer between 1964 and 1970.

On the other hand, calculations of the possible modulation of stratospheric ozone due to the penetration variability in the atmosphere of galactic cosmic rays [*Ruderman and Chamberlain,* 1975] and the related formation of nitrogen oxides in the lower stratosphere, mainly at high latitude [*Warneck,* 1972; *Nicolet and Peetermans,* 1972; *Brasseur and Nicolet,* 1973; *Nicolet,* 1975*a, b*] have been performed. Our model shows that this effect can be neglected in comparison with the ozone modulation due to UV variability as adopted in this work.

Finally, the corresponding changes in the heating rate by O_3 absorption and in the temperature distribution as determined by our 2-D model are shown respectively in Figures 10 and 11. The temperature increases with solar flux mainly above 30 km because of the enhanced ozone heating by UV fluxes. The effect which is most significant in the equatorial and tropical regions must be related to the meridional distribution of the ozone variation (Figure 9). A comparison with the results obtained by *Callis and Nealy* [1978*a, b*] and, to a

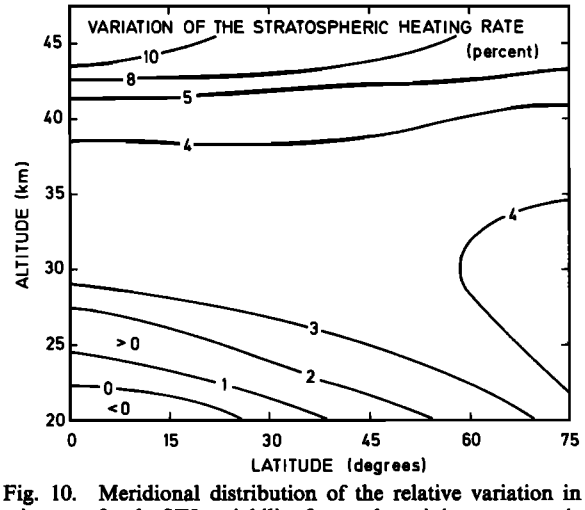

Fig. 10. Meridional distribution of the relative variation in the heating rate for the UV variability from solar minimum to maximum (Figure 2).

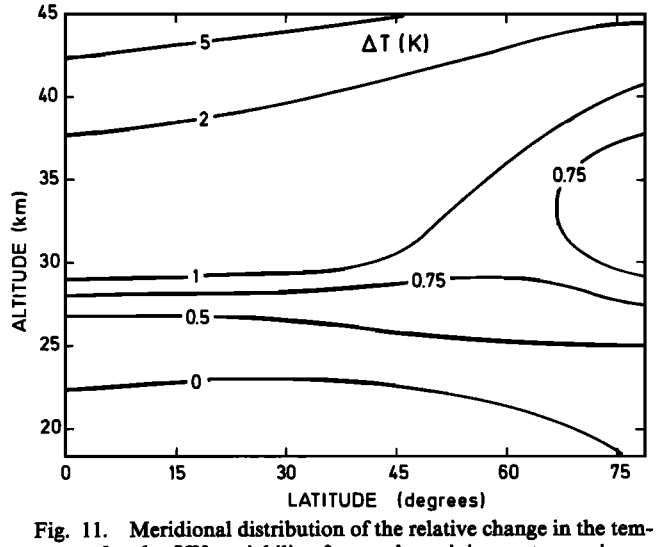

Fig. 11. Meridional distribution of the relative change in the temperature for the UV variability from solar minimum to maximum (Figure 2).

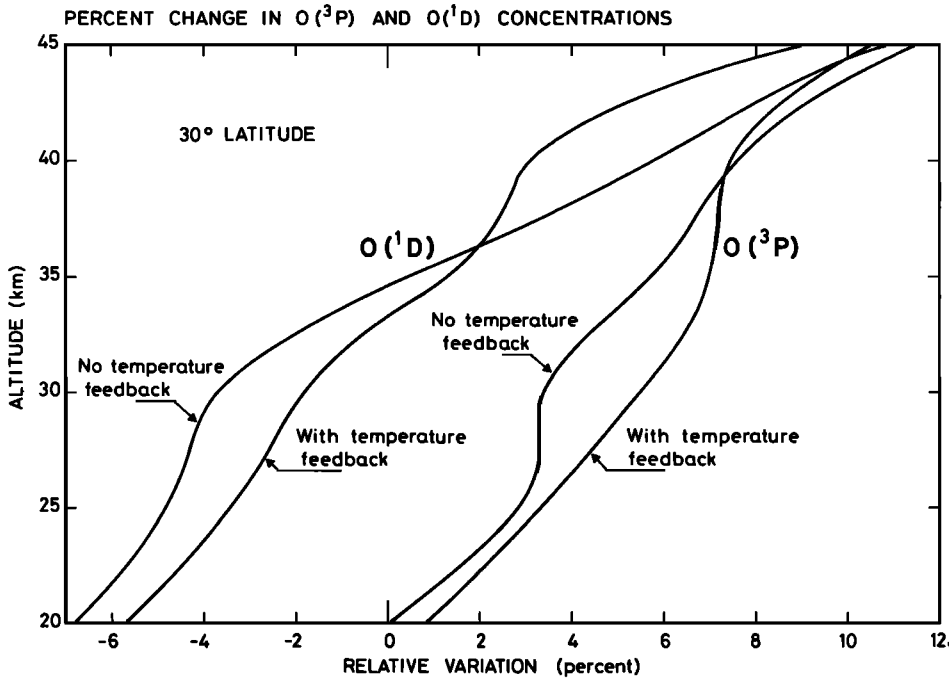

Fig. 12. Vertical distribution of the relative change in the average atomic oxygen concentration at 30 degrees latitude for the UV variability from solar minimum to maximum (Figure 2).

certain extent, by *Penner and Chang* [1978] indicate that the temperature variation values obtained by these authors are significantly larger than ours.

It should also be noted that *Callis and Nealy* [1978*b*] have derived a negative variation of the ozone concentration in the upper stratosphere while the results obtained by *Callis and Nealy* [1978*a*], by *Penner and Chang* [1978] and by ourselves show a positive variation. The difference may be mainly due to the magnitude of the temperature change which as mentioned is much larger in the results of *Callis and Nealy* [1978*b*].

The stratospheric temperature trends observed since the 1960's have been analyzed by different authors [*Angell and Korshover*, 1978*b*; *Quiroz*, 1979]. The warming occurring prior to 1970 in the middle and upper stratosphere and the cooling recorded in the beginning of the 1970's shows a high correlation with solar cycle 20 as quoted by *Quiroz* [1979]. This author has indicated that the corresponding temperature change from solar maximum (1969) to solar minimum (1975) varies among the stations from −3°C to −6°C in the upper stratosphere. These values are in fairly good agreement with our results at 45 km which provide a variation of 6°C at the equator and 3°C at 60 degrees. However, below 40 km, the computed

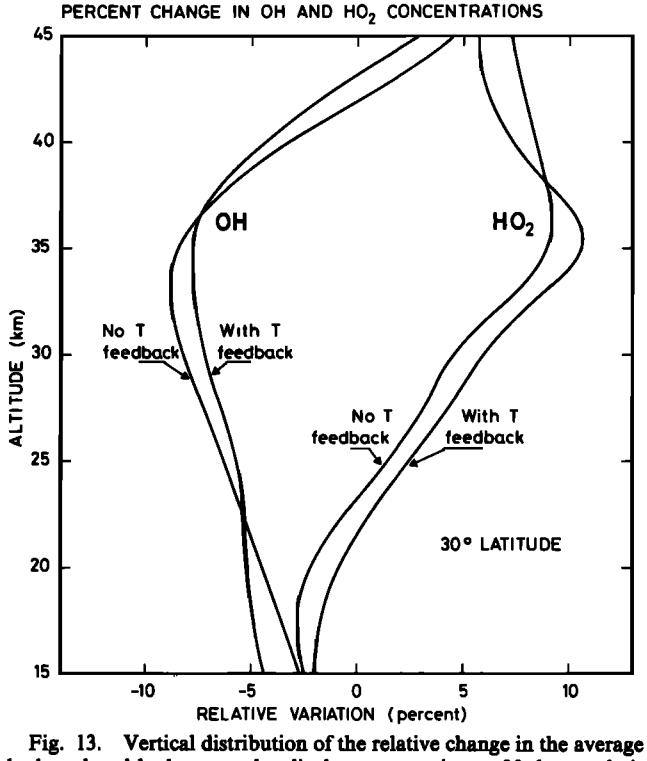

Fig. 13. Vertical distribution of the relative change in the average hydroxyl and hydroperoxyl radicals concentration at 30 degrees latitude for the UV variability from solar minimum to maximum (Figure 2).

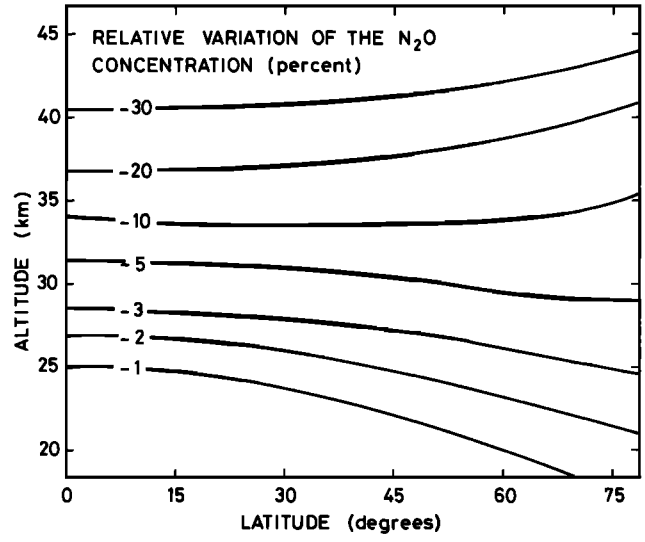

Fig. 14. Meridional distribution of the relative change in the nitrous oxide concentration for the UV variability as represented in Figure 2. Temperature feedback taken into account.

temperature change seems smaller than the observations. Moreover, the variations reported by *Quiroz* [1979] appears to be fairly uniform among most stations while our results show some latitudinal variations.

The effect of the UV variability on atomic oxygen is illustrated in Figure 12. The enhancement at high altitude of the concentration associated with a higher solar flux value is due, for $O(^3P)$ and $O(^1D)$, to the increased concentration of ozone and to the increased rate of its photodissociation. In the lower stratosphere, the negative change of the $O(^1D)$ concentration is due to the increased absorption of UV radiation by ozone, the concentration of which becomes larger at higher altitudes.

The percentage change of the hydroxyl and hydroperoxyl radicals concentration is represented in Figure 13. This graph shows a global increase with altitude of the HO_x variation, which can be explained by a similar increase of the $O(^1D)$ variation with height. The presence of OH and HO_2 radicals in the stratosphere is primarly due to the oxidation of water vapir, methane and molecular hydrogen by $O(^1D)$ atoms. As stated above, the water vapor is held constant in the model. However had water vapor been allowed to vary, there would have been a small increase of H_2O [*Penner and Chang*, 1980] due to more oxidation of methane. This should lead to an increase of the OH and HO_2 concentration in the upper stratosphere and consequently for OH to a lower crossover point from negative to positive variations. These changes should have a limited impact on the ClO/HCl concentration ratio but the effect on ozone is not expected to be large.

The change in the HO_2 to OH ratio, which also appears, is related to the variation of O_3, $O(^3P)$, NO and CO which determines the value of this ratio. Near the stratopause, one can see that the factor $n(HO_2)/n(OH)$ remains unchanged since it becomes almost independent of any concentration.

The relative variation of long lived species produced at ground level such as N_2O, CCl_4, $CFCl_3$ and CF_2Cl_2 is illustrated in Figures 14 and 15 assuming for these constituents a fixed concentration at ground level and steady state conditions. In both cases, large perturbations are obtained but these occur at high altitude where the concentration becomes relatively small. Nevertheless, the long term measurement of the concentration of such species around 40 km should give an indication of the real existence of a solar variability associated with the 11-year cycle. For N_2O, CCl_4, $CFCl_4$ and CF_2Cl_2, the

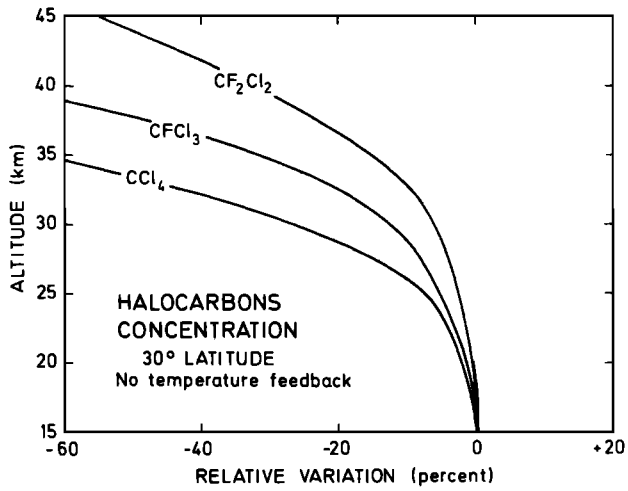

Fig. 15. Vertical distribution at 30 degrees latitude of the relative change in the concentration of CCl_4, $CFCl_3$, and CF_2Cl_2 from solar minimum to maximum (Figure 2).

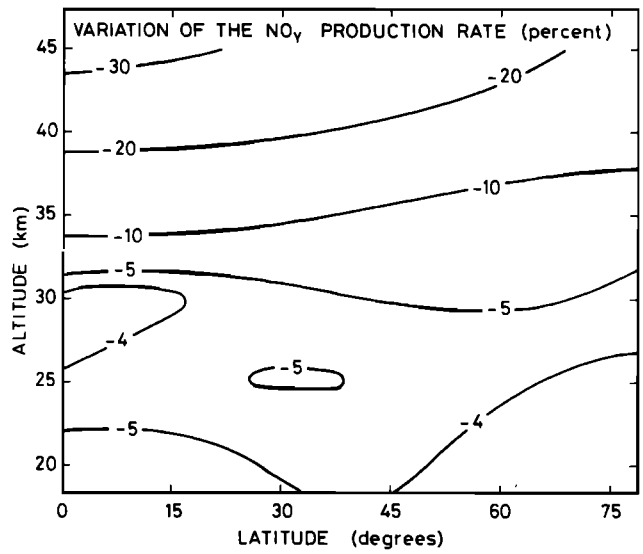

Fig. 16. Meridional distribution of the change in the nitric oxide production rate for the UV variability from solar minimum to maximum (Figure 2). Temperature feedback taken into account.

negative variation computed in the model is due to the increase in the photodissociation rate of these molecules. However, the production rate of ClX which is the product of the dissociation coefficient and the concentration of halocarbons (varying with opposite signs) varies locally much less and its integrated value remains unchanged if the flux at ground level is kept constant (atmospheric release of chlorofluorocarbons). Moreover it should be noted that CH_3Cl, the most important producer of ClX in the natural stratosphere, is positively correlated with the UV flux since its main destruction is due to the reaction with hydroxyl radicals OH which are slightly depleted when the solar irradiance increases. The same effect appeas for methane. The calculations referring to ClO and HCl indicate that the average concentration varies in both cases by less than 4%.

Odd nitrogen in the stratosphere is formed by the reaction between N_2O and $O(^1D)$. The variation in the corresponding production rate, illustrated in Figure 16, is negative and yields

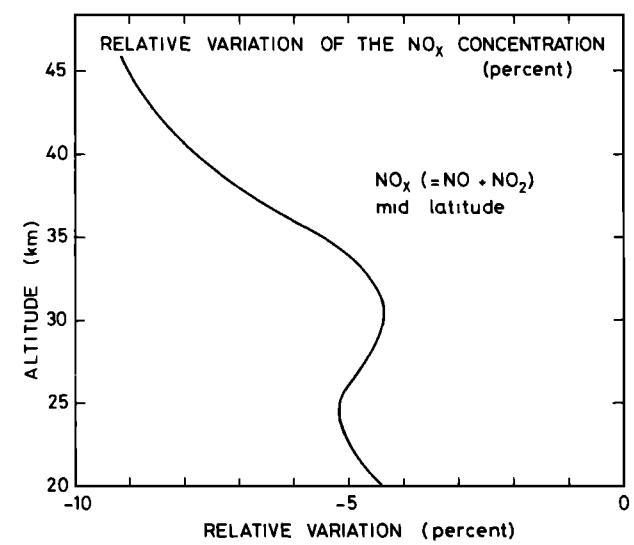

Fig. 17. Vertical distribution of the relative change in the NO_x (NO + NO_2) concentration at 30 degrees latitude for the UV variability from solar minimum to solar maximum (Figure 2). Temperature feedback taken into account.

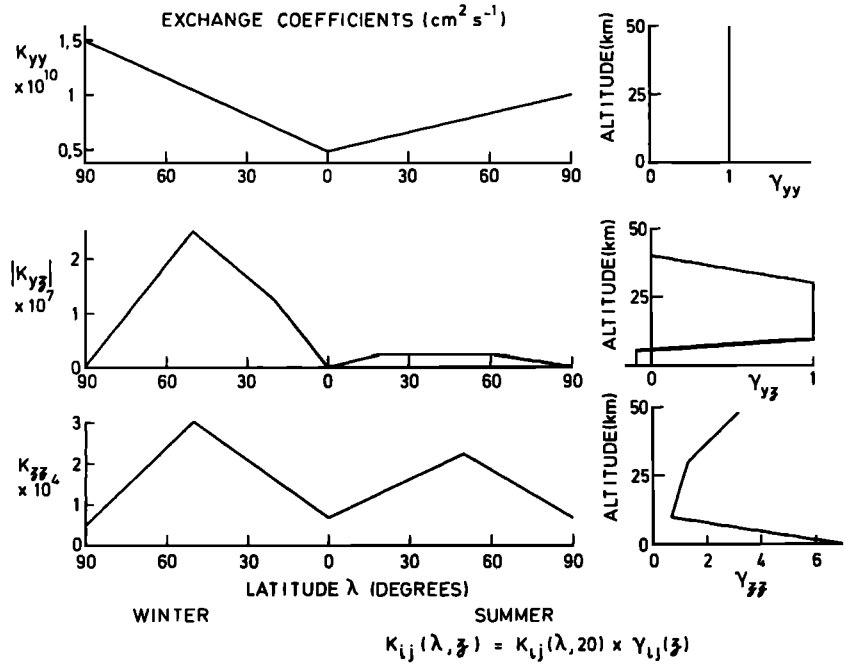

Fig. A1. Distribution of the exchange coefficients versus latitude and altitude adopted after adjustment in the time dependent version of the model.

30% above 44 km in the equatorial region. Therefore, the decrease of the NO_x concentration (Figure 17) can be significant mainly in the upper stratosphere and should contribute to increase the ozone concentration in this region.

5. Concluding Remarks

There are indications that the UV irradiance responsible for the photodissociation of several minor constituents and for the local heating in the stratosphere, shows time variations related to the 11-year solar cycle. However the variability suggested by *Heath and Thekaekara* [1977] seems to be overestimated if a critical analysis of the solar irradiance measurements is performed. Therefore a more realistic dependence on wavelength, based on several observations including recent balloon measurements, is suggested.

If such a variation is applied to the stratospheric photochemical and thermal calculations, a total ozone variation of the order of 3% from the minimum to the maximum solar activity should be expected. The largest change, namely 10% when the temperature feedback is taken into account, appears in the upper stratosphere. The corresponding calculations with the solar flux variability of *Heath and Thekaekara* [1977] lead to ozone variations (24% at 45 km and 30 degrees) which should be detected with the current ozone network. However, the best estimates of the ozone amount made between 1957 and 1975 (see, e.g., the analysis of *Angell and Korshover* [1973, 1976, 1978*a*] provide no unambiguous evidence that total ozone varies significantly with solar cycle. H. U. Dütsch (personal communication, 1979), has reported such a possible correlation with a time lag of the order of 2 years, but his analysis is based on the data from a single station, namely, Arosa in Switzerland. Consequently, the solar flux variability suggested in this work seems to be more acceptable than the values proposed earlier and, with the data presently available, should even be considered as an upper limit. In fact if there is a long-term variability in the solar irradiance, it should appear in the behavior of more sensitive species such as N_2O. Therefore a monitoring of this gas in the upper stratosphere should give unambiguous information concerning the possible existence of solar flux variability. Finally long-term observation of the UV irradiance is required since the response of the stratosphere to anthropogenic perturbations cannot be carefully studied without considering the natural variability of the various trace species.

Appendix: Description of the IAS 2-D Model

Introduction

The IAS 2-D model has been constructed to investigate the structure of the natural atmosphere and to study the behavior of stratospheric minor constituents [*Brasseur*, 1978*a*, *b*; *Brasseur and Bertin*, 1974, 1977, 1978]. It can be run for several conditions, namely: (1) in a steady state version with an over-

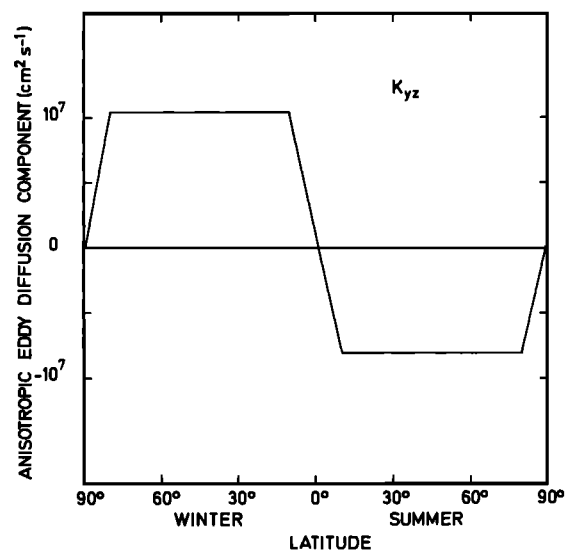

Fig. A2. Latitudinal distribution of K_{yz} (absolute value) adopted below 25 km in the steady state model.

TABLE 4*a*. Principal Chemical Reactions in the Stratosphere and Their Rate Constants

Reaction	Rate Constant, $cm^3\ s^{-1}$	Reference
$O + O + M \rightarrow O_2 + M$	$k_1 = 4.7 \times 10^{-33} (300/T)^2\ n(M)$	*Nicolet* [1975*a*, *b*]
$O + O_2 + M \rightarrow O_3 + M$	$k_2 = 1.1 \times 10^{-34}\ e^{510/T}\ n(M)$	*Hampson and Garvin* [1978]
$O + O_3 \rightarrow O_2 + O_2$	$k_3 = 1.9 \times 10^{-11}\ e^{-2300/T}$	*Hampson* [1973]
$O(^1D) + N_2 \rightarrow O(^3P) + N_2$	$k_4 = 2.0 \times 10^{-11}\ e^{107/T}$	*Davidson et al.* [1977]
$O(^1D) + O_2 \rightarrow O(^3p) + O_2$	$k_5 = 2.9 \times 10^{-11}\ e^{67/T}$	*Davidson et al.* [1977]
$H + O_2 + M \rightarrow HO_2 + M$	$a_1 = 2.1 \times 10^{-32}\ e^{290/T}\ n(M)$	*Wong and Davis* [1974]
$H + O_3 \rightarrow O_2 + OH_{v\leq 9}$*	$a_2 = 1.0 \times 10^{-10}\ e^{-516/T}$	*Clyne and Monkhouse* [1977]
$OH + O \rightarrow H + O_2$	$a_5 = 4.0 \times 10^{-11}$	Working value, cf. *Wilson* [1972]
$OH + O_3 \rightarrow HO_2 + O_2$	$a_6 = 1.5 \times 10^{-12}\ e^{-1000/T}$	*NASA* [1977]
$HO_2 + O_3 \rightarrow OH + 2O_2$	$a_{6b} = 1.4 \times 10^{-14}\ e^{-580/T}$	*NASA* [1979]
$HO_2 + O \rightarrow O_2 + OH_{v\leq 6}$*	$a_7 = 3.5 \times 10^{-11}$	*Burrows et al.* [1977]
$O(^3P) + NO_2 \rightarrow NO + O_2$	$b_3 = 9.1 \times 10^{-12}$	*Davis et al.* [1973*a*, *b*]
$O_3 + NO \rightarrow NO_2 + O_2$	$b_4 = 2.1 \times 10^{-12}\ e^{-1450/T}$	*NASA* [1977]
$N(^4S) + NO \rightarrow N_2 + O$	$b_6 = 8.2 \times 10^{-11}\ e^{-410/T}$	*Clyne and McDermid* [1975]
$N(^4S) + O_2 \rightarrow NO + O$	$b_7 = 5.5 \times 10^{-12}\ e^{-3200/T}$	*Becker et al.* [1969]
$NO_2 + O_3 \rightarrow NO_3 + O_2$	$b_9 = 1.2 \times 10^{-13}\ e^{-2450/T}$	*NASA* [1977]
$NO_3 + NO_2 + M \rightarrow N_2O_5 + M$	$b_{12} = 2.8 \times 10^{-30}\ n(M)$ $= 3.8 \times 10^{-12}$ (limiting value)	*Baulch et al.* [1973]
$NO_2 + OH + M \rightarrow HNO_3 + M$	b_{22} (see below)	*NASA* [1977]
$HNO_3 + OH \rightarrow H_2O + NO_3$	$b_{27} = 9 \times 10^{-14}$	*Margitan et al.* [1975]
$N_2O_5 + M \rightarrow NO_3 + NO_2 + M$	$b_{32} = 2.2 \times 10^{-5}\ e^{-9700/T}$ $= 5.7\ 10^{14}\ e^{-10600/T}$ (limiting value) of $b_{32}n(M)$	*Baulch et al.* [1973]
$N_2O + O(^1D) \rightarrow N_2 + O_2$	$b_{38} = 5.5 \times 10^{-11}$	*Davidson et al.* [1977]
$N_2O + O(^1D) \rightarrow 2NO$	$b_{39} = 5.5 \times 10^{-11}$	*Cvetanovic* [1974]
$HO_2 + NO_2 + M \rightarrow HO_2NO_2 + M$	$b_{23} = 7.5 \times 10^{-33}\ e^{+1000/T}\ n(M) \times \frac{1}{1 + 4.9 \times 10^{-12}\ [n(M)]^{0.61}}$	*Howard* [1978]
$OH + OH \rightarrow H_2O + O$	$a_{16} = 1 \times 10^{-11}\ e^{-550/T}$	*Baulch et al.* [1972]
$OH + HO_2 \rightarrow H_2O + O_2$	$a_{17} = 3 \times 10^{-11}$	*NASA* [1977]
$H + HO_2 \rightarrow OH + OH$	$a_{23a} = 4.2 \times 10^{-10}\ e^{-950/T}$	*Baulch et al.* [1972]
$H + HO_2 \rightarrow H_2O_2$	$a_{23b} = 4.2 \times 10^{-11}\ e^{-350/T}$	*Baulch et al.* [1972]
$H + HO_2 \rightarrow H_2O + O$	$a_{23c} = 8.3 \times 10^{-11}\ e^{-500/T}$	*Lloyd* [1974]
$H_2 + O(^3P) \rightarrow OH + H$	$a_{24} = 8.8 \times 10^{-12}\ e^{-4200/T}$	*Dubinsky and McKenney* [1975]
$HO_2 + NO \rightarrow NO_2 + OH$	$a_{26} \equiv b_{29} = 3.3 \times 10^{-12}\ e^{254/T}$	
$HO_2 + HO_2 \rightarrow H_2O_2 + O_2$	$a_{27} = 2.5 \times 10^{-12}$	*Hamilton and Lii* [1977]
$OH + CO \rightarrow CO_2 + H$	$a_{36} = 1.4 \times 10^{-13}$	*NASA* [1977]
$O(^1D) + H_2O \rightarrow OH + OH$	$a_1^* = 2.3 \times 10^{-10}$	*Davidson et al.* [1977]
$O(^1D) + CH_4 \rightarrow CH_3 + OH$	$a_2^* = 1.4 \times 10^{-10}$	*Davidson et al.* [1977]
$O(^1D) + H_2 \rightarrow OH + H$	$a_3^* = 1.0 \times 10^{-10}$	*Davidson et al.* [1977]
$CH_4 + OH \rightarrow CH_3 + H_2O$	$c_2 = 2.36 \times 10^{-12}\ e^{-1710/T}$	*Davis et al.* [1973*a*]
$CH_3O_2 + NO \rightarrow CH_3O + NO_2$	$c_5 = 3.3 \times 10^{-12}\ e^{-500/T}$	*Demerjian et al.* [1974]
$CH_3Cl + OH \rightarrow CH_2Cl + H_2O$	$d_1 = 2.2 \times 10^{-12}\ e^{-1142/T}$	*NASA* [1977]
$Cl + O_3 \rightarrow ClO + O_2$	$d_2 = 2.7 \times 10^{-11}\ e^{-257/T}$	*Watson* [1977]
$ClO + O \rightarrow Cl + O_2$	$d_3 = 7.7 \times 10^{-11}\ e^{-130/T}$	*NASA* [1977]
$ClO + NO \rightarrow Cl + NO_2$	$d_4 = 1.0 \times 10^{-11}\ e^{+200/T}$	*NASA* [1977]
$Cl + CH_4 \rightarrow HCl + CH_3$	$d_5 = 7.3 \times 10^{-12}\ e^{-1260/T}$	*Watson* [1977]
$Cl + HO_2 \rightarrow HCl + O_2$	$d_7 = 3 \times 10^{-11}$	*Leu and DeMore* [1976]
$HCl + OH \rightarrow Cl + H_2O$	$d_{11} = 3 \times 10^{-12}\ e^{-425/T}$	*Watson* [1977]
$ClO + NO_2 + M \rightarrow ClONO_2 + M$	d_{22} see below $d_{22} = \frac{3.3 \times 10^{-23}\ T^{-3.34}\ n(M)}{1 + 8.7 \times 10^{-9}\ T^{-0.6}\ [n(M)]^{0.5}}$	*Zahniser et al.* [1977]
$ClONO_2 + O \rightarrow$ products	$d_{32} = 3 \times 10^{-12}\ e^{-808/T}$	*NASA* [1977]
$ClO + HO_2 \rightarrow HOCl + O_2$	$d_{35} = 4.5 \times 10^{-12}$	*Howard* [1978]

simplified transport parameterization; this version has been used in the present work since it is not highly time consuming; (2) in a time-dependent version with a less detailed chemistry but a more elaborated transport representation.

Physical Domain and Equations

The physical domain of the model extends from the ground (0 km) to the stratopause (50 km) and from the north pole (+90°) to the south pole (−90°). For each constituent i (or family of constituents—see below), one solves a continuity equation, namely,

$$[v]\frac{\partial n_i}{a\partial\phi} + [w]\left\{\frac{\partial [n_i]}{\partial z} + \frac{[n_i]}{H}\right\} + \frac{1}{a\cos\phi}\frac{\partial}{\partial\phi}[n_i^*\, v_i^*]\cos\phi + \frac{\partial}{\partial z}[n_i^* w_i^*] = [P_i] - [L_i] \quad (1)$$

TABLE 4b. Parameters for an Analytical Expression for the Second-Order Rate Constant of the Reaction $HO + NO_2(+ N_2) \rightarrow HONO_2(+ N_2)$ [*NASA*, 1977]

$$\log (b_{22}) = -AT/(B + T) - 0.5 \log_{10} (T/280)$$
$$A = A_1 + A_2Z + A_3Z^2 + A_4Z^3$$
$$B = B_1 + B_2Z + B_3Z^2$$
$$A_1 = 31.62273$$
$$A_2 = -0.258304$$
$$A_3 = -0.0889287$$
$$A_4 = 2.520173 \times 10^{-3}$$
$$B_1 = -327.372$$
$$B_2 = 44.5586$$
$$B_3 = -1.38092$$

Where $Z = \log_{10} [N_2]$ and is applicable only for the range $200 < T/K < 350$ and $16.3 < \log_{10} ([N_2]/\text{molecule cm}^{-3}) < 19.5$, with an estimated reliability in log k of ± 0.10 (reliability analogous to 1σ). Air is approximately 6% less efficient than nitrogen as a third body (i.e., the expression above may be used with $[Air] = 0.94\ [N_2]$).

where n_i is the concentration of species i, v and w the meridional and vertical wind components, respectively, H the atmospheric scale height, ϕ the latitude, z the altitude, a the Earth's radius, P_i and L_i the production and the loss rates, respectively. The brackets refer to zonal mean variables and the asterisks to the deviations from this average.

The components of the wind related to the mean general circulation are prescribed as fixed parameters. The wave or eddy components are parameterized in the model using the generalized diffusion equation suggested by *Demazure and Saïssac* [1962] and *Reed and German* [1965]:

$$[n_i^* v_i^*] = -n(M) \left[K_{yy} \frac{\partial [f_i]}{a \partial \phi} + K_{yz} \frac{\partial [f_i]}{\partial z} \right] \quad (2a)$$

$$[n_i^* w_i^*] = -n(M) \left[K_{zy} \frac{\partial [f_i]}{a \partial \phi} + K_{zz} \frac{\partial [f_i]}{\partial z} \right] \quad (2b)$$

where $f_i = n_i/n(M)$ is the volume mixing ratio and $n(M)$ the total atmospheric concentration.

The transport parameters used in the model differ from one version to another. In the time dependent approach, the wind components are usually taken from *Cunnold et al.* [1975]. The distribution of the exchange coefficients (K_{ij}) are based on the shape of the profiles given by *Gudiksen et al.* [1968] and *Luther* [1973] but are adjusted by a 'trial and error' method

TABLE 5. Principal Photochemical Reactions in the Stratosphere

$$O_2 + h\nu \rightarrow O + O$$
$$O_3 + h\nu \rightarrow O(^3P) + O_2$$
$$O_3 + h\nu \rightarrow O(^1D) + O_2$$
$$NO_2 + h\nu \rightarrow NO + O$$
$$HNO_3 + h\nu \rightarrow NO_2 + OH$$
$$N_2O + h\nu \rightarrow N_2 + O$$
$$N_2O_5 + h\nu \rightarrow NO_2 + NO_3$$
$$CH_3Cl + h\nu \rightarrow CH_3 + Cl$$
$$CFCl_3 + h\nu \rightarrow CFCl_2 + Cl$$
$$CF_2Cl_2 + h\nu \rightarrow CF_2Cl + Cl$$
$$CCl_4 + h\nu \rightarrow CCl_3 + Cl$$
$$HCl + h\nu \rightarrow H + Cl$$
$$ClONO_2 + h\nu \rightarrow ClO + NO_2$$

[*Brasseur*, 1980] to give the best agreement between the observed and calculated ozone distribution. In order to facilitate the determination of the K values, it is assumed that they can be expressed as a function of latitude (ϕ) alone multiplied by a function of height (z) alone (variable separation):

$$K_{ij}(\phi, z) = K_{ij}(\phi, 20 \text{ km}) \times \gamma_{ij}(z) \quad (3)$$

Figure A1 shows the result of this calibration.

In the steady state version of the model, oversimplified transport conditions are adopted. The mean circulation is not considered while the eddy diffusion components distribution are kept simple. K_{yy} and K_{zz} are constant in the whole domain and equal to 10^{10} cm^2 s^{-1} and 10^4 cm^2 s^{-1}, respectively. K_{yz} is adjusted until the meridional distribution of ozone becomes realistic (see Figure A2). It is interesting to note that such a elementary parameterization leads to distributions of chemical species which are in rather good agreement with the observation or with the results obtained when a more elaborated transport representation is adopted.

The meridional distribution of the temperature is derived from the energy equation

$$[v] \frac{\partial [\theta]}{a \partial \phi} + [w] \frac{\partial [\theta]}{\partial z} + \frac{1}{a \cos \phi} \frac{\partial}{\partial \phi} ([v^* \theta^*] \cos \phi) + \frac{\partial}{\partial z} [w^* \theta^*] - \frac{[w^* \theta^*]}{H} = \frac{[Q]}{\rho C_p} \left(\frac{p_0}{p} \right)^\kappa$$

where

$$\theta = T(p_0/p)^\kappa$$

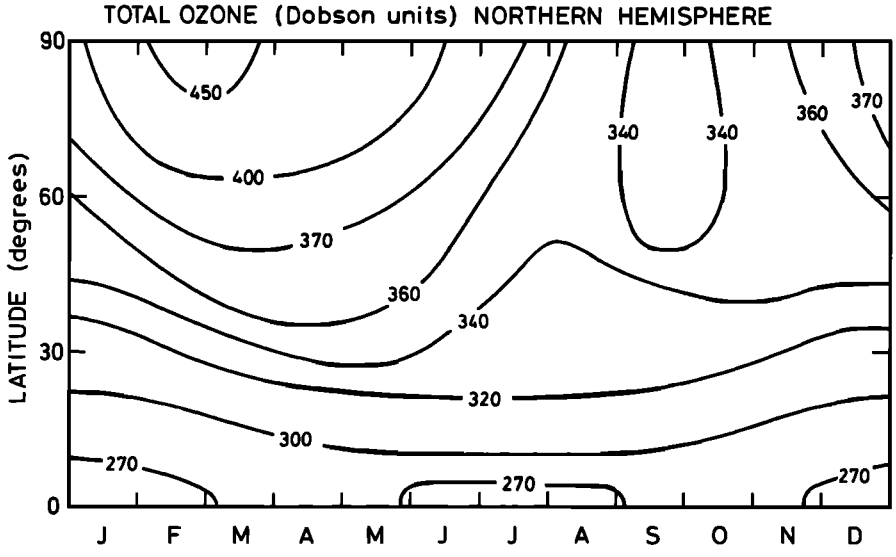

Fig. A3. Predicted distribution of total ozone as a function of month and latitude.

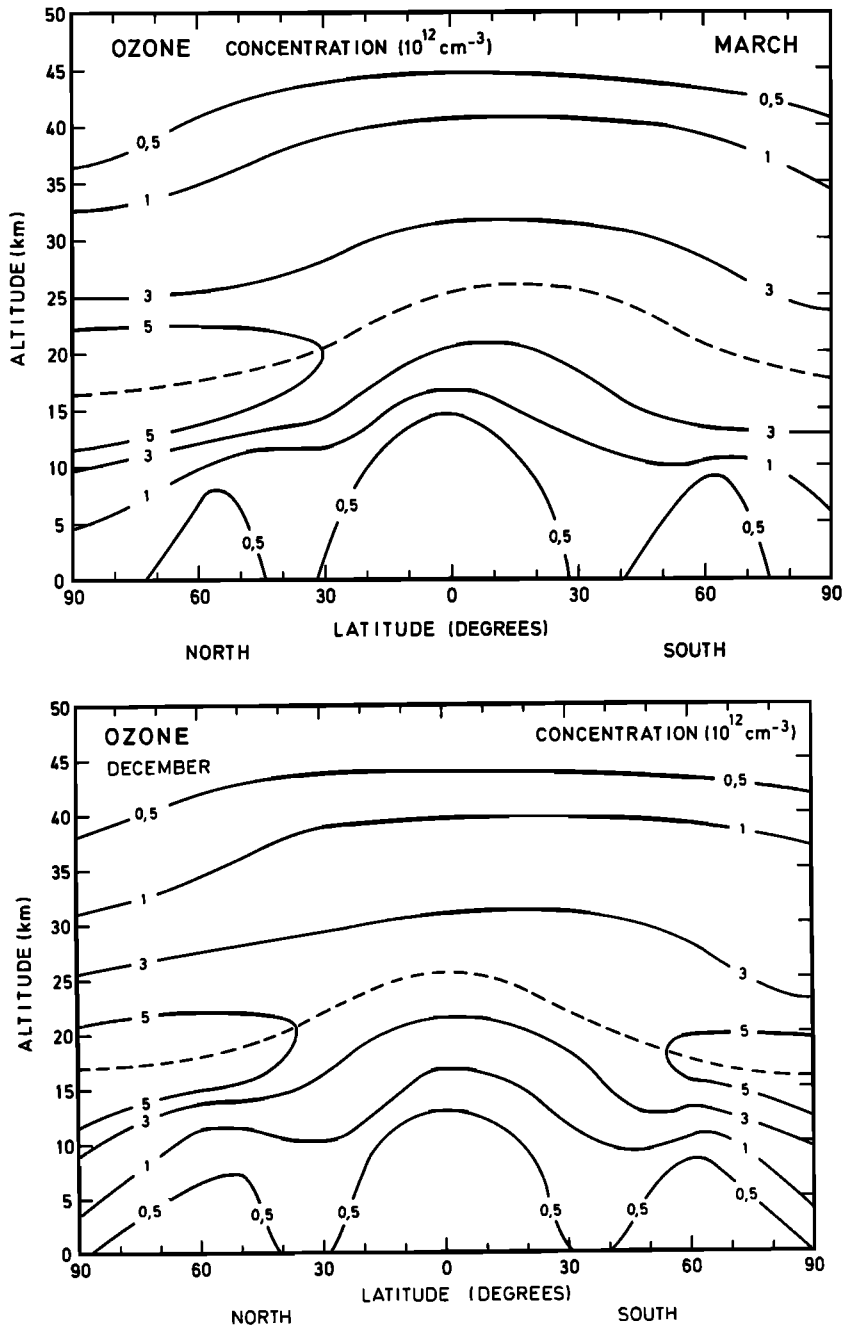

Fig. A4. Meridional cross section of the ozone concentration in March and December.

is the potential temperature, p the atmospheric pressure, p_0 = 1000 mbar, κ the factor R/C_p, R the perfect gas constant, C_p the specific heat at constant pressure and ρ the atmospheric mass density. Q is the net heating rate which is related to the UV absorption or IR emission by chemical species.

Above 30 km, the heating due to the absorption of UV radiation by the Hartley and Huggins bands of ozone is calculated explicitly while the infrared cooling related to the emission mainly by carbon dioxide (15 μm) and by ozone (9.6 μm) is parameterized by means of the empirical relation of *Dickinson* [1973]:

$$Q = n(O_3) \int_\nu \varepsilon_\nu(z, \chi)\, \sigma_\nu\, d\nu - [L_{ref}(z) + a(z)(T(\phi, z) - T_{ref}(z))]$$

where $n(O_3)$ is the local ozone concentration, ε_ν the solar energy at the frequency ν, altitude z and solar zenith angle χ, and $\sigma_\nu(O_3)$ the absorption cross section of ozone. $L_{ref}(z)$ is the cooling rate calculated by *Dickinson* [1973] in a reference 1-D atmosphere with a temperature profile $T_{ref}(z)$. $T(\phi, z)$ is the actual temperature at latitude ϕ and altitude z and $a(z)$ is a Newtonian cooling coefficient which is also determined as a function of the altitude by *Dickinson* [1973]. In the lower stratosphere and in the troposphere where the heating by ozone becomes negligible, the effect of latent heat becomes significant. Therefore, below 20 km, the net heating rate is parameterized by the following expression suggested by *Trenberth* [1973]:

$$\frac{Q}{\rho C_p} = h(z)[T^*(\phi, z) - T(\phi, z)]$$

where $h(z)$ is a Newtonian cooling coefficient including boundary layer heating and latent heat release, and $T^*(\phi, z)$ is

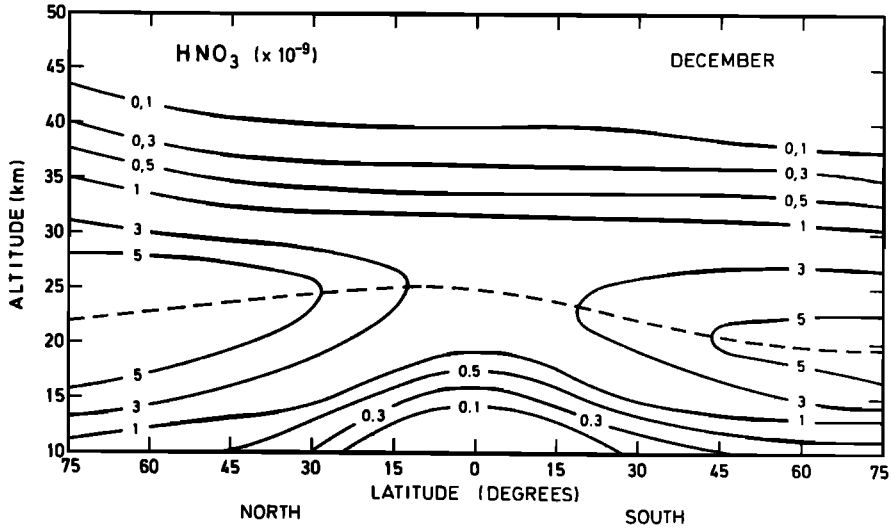

Fig. A5. Meridional cross-section of the nitric acid volume mixing ratio obtained with the time dependent version of the model.

an average equilibrium temperature obtained from data. Between 20 and 30 km a linear combination of both methods is used. The turbulent transport of heat is represented by

$$[v^*\theta^*] = -\left\{K_{yy}\frac{\partial[\theta]}{a\partial\phi} + K_{yz}\frac{\partial[\theta]}{\partial z}\right\}$$

$$[w^*\theta^*] = -\left\{K_{zy}\frac{\partial[\theta]}{a\partial\phi} + K_{zz}\frac{\partial[\theta]}{\partial z}\right\}$$

The exchange coefficients for heat transport are of the same order of magnitude as the coefficients related to the transport of chemical species but have not always the same value.

Chemical Species

The chemical and photochemical scheme used in the model (Tables 4 and 5) results from the analysis of stratospheric reactions made by several authors [e.g., *Nicolet, 1975a, b*] or working groups [e.g., *NASA, 1977*].

In order to avoid numerical instability problems due to the stiffness of the system and to facilitate the use of large time-step when integrating the equations, species are grouped into families ($O_x = O_3 + O(^3P) + O(^1D)$; $NO_y = NO + NO_2 + 2N_2O_5 + HNO_3 + ClONO_2$; $ClX = Cl + ClO + ClONO_2 + HCl$) and the continuity equations for these families are solved taking into account the transport effect and their external production and loss rates. The concentration of the individual species is then derived assuming local photochemical equilibrium between the constituents belonging to a specified family.

The average value of the solar flux over 24 hours $\bar{q}$ is approximated by a two points discretisation as suggested by the MIT group. [*Cunnold et al., 1975*]

$$\bar{q} = \frac{\mathscr{H}}{2\pi}\left[q\left(AH = \frac{\mathscr{H}}{4}\right) + q\left(AH = \frac{3\mathscr{H}}{4}\right)\right]$$

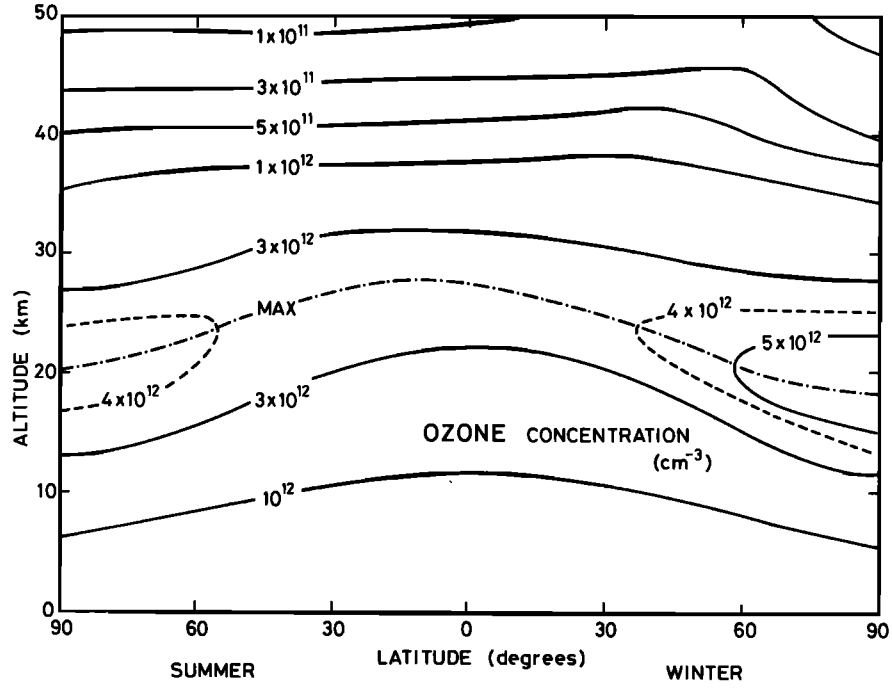

Fig. A6. Meridional cross section of the ozone concentration obtained with the steady state version of the model.

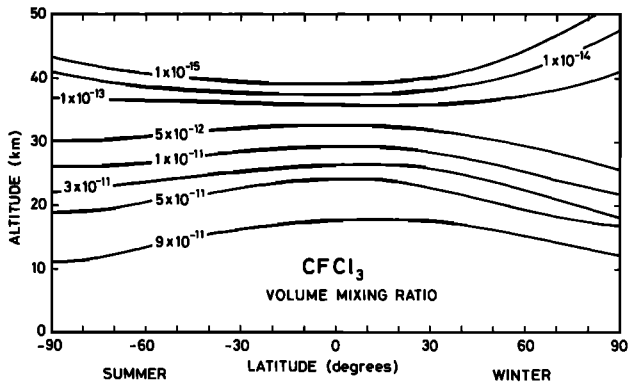

Fig. A7. Meridional cross section of the $CFCl_3$ volume mixing ratio obtained with the steady state version of the model.

where AH is the solar hour angle, $\mathscr{H}$ is the value of AH at sunset (or sunrise) and is given by

$$\cos \mathscr{H} = -tg\ \phi\ tg\ \delta$$

where ϕ is the latitude and δ the solar declination. In the steady state version δ is chosen to be equal to -10 degrees while in the time-dependent version δ varies with season from -23 degrees to $+23$ degrees. In this case the flux is recomputed every 15 days.

Boundary Conditions

A zero horizontal flux of all trace species at the north (winter) and the south (summer) pole is assumed so that the zonal symmetry around the terrestrial axis is respected. At the ground and at stratopause level, a fixed concentration is speci-

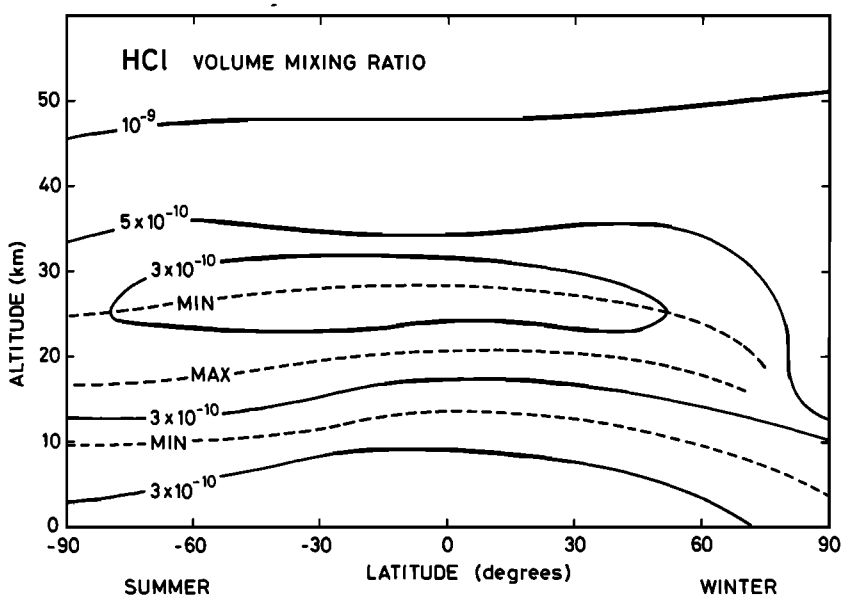

Fig. A8. Meridional cross section of the HCl volume mixing ratio obtained with the steady state version of the model.

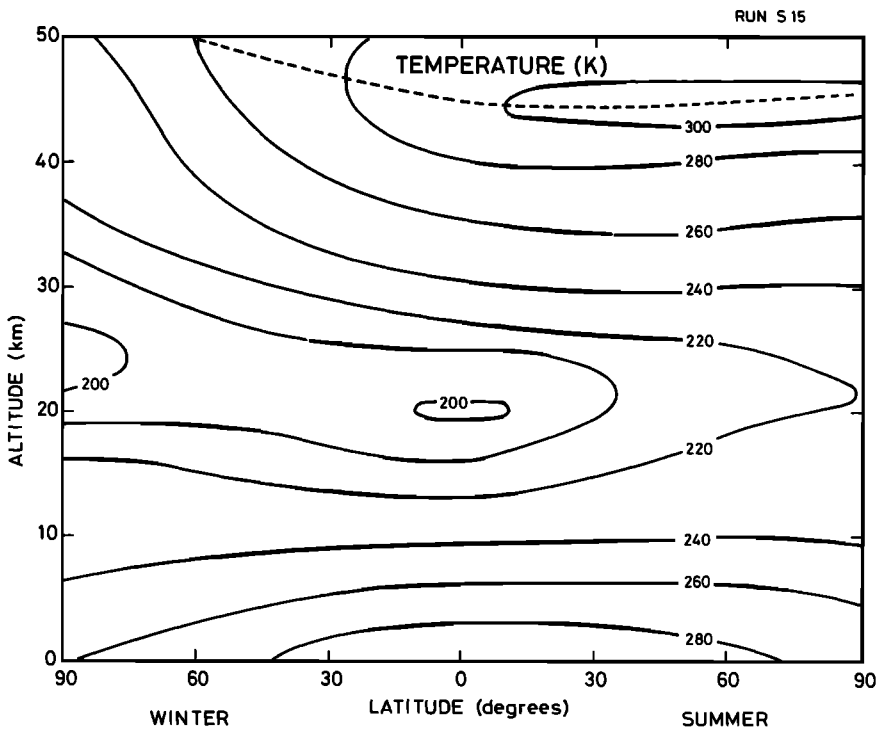

Fig. A9. Meridional cross section of the temperature obtained with the steady state version of the model.

fied [*Brasseur and Bertin*, 1978]. Most of the conditions at the upper boundary are based on the results provided by 1-D models which extend to higher altitudes. The lower condition related to chlorofluorocarbons is representative of a 1980 situation. It should be noted that this type of boundary condition implies that the chlorine flux into the model may be a function of the internal chemistry and therefore of the UV irradiance. However, since the tropospheric photodissociation of the chlorofluorocarbons is very weak, the change in the flux at ground level is small and the type of condition at ground level adopted here does not considerably influence the global picture of the results. Nevertheless further investigations of this question are required.

Numerical Treatment

The problem is treated numerically by approximating the space derivations by finite differences and by solving the system which is obtained using an alternating directions method [*Peaceman and Rachford*, 1955]. The grid spacing is 1 km in the vertical and 5 degrees (~550 km) in the horizontal. In the time-dependent version of the model, the time-step is usually choosen to be 1–5 days. The continuity equations related to the various species are treated successively and an iteration is performed in the steady state version until equilibrium conditions are reached.

Selected Results

Different simulations of the natural atmosphere have been undertaken with the various versions of the model. A typical evolution of total ozone at various latitudes is given in Figure A3, while Figures A4*a* and A4*b* represent the meridional distribution of O_3 in March and December and Figure A5 the similar results for nitric acid in December. Figure A6 shows the distribution of the ozone concentration obtained with the steady state version of the model and Figures A7 and A8 the similar results for $CFCl_3$ and HCl.

Finally, Figure A9 depicts the meridional distribution of the temperature as computed with the steady state model.

Acknowledgments. The authors are indebted to C. Nicolis for her collaboration in developing the thermal scheme used in this work. They also thank P. De Baets for his help in the numerical treatment of this problem.

REFERENCES

Angell, J. K., and J. Korshover, Quasi-biennial and long-term fluctuations in total ozone, *Mon. Weather Rev., 101,* 426, 1973.

Angell, J. K., and J. Korshover, Global analysis of recent total ozone fluctuations, *Mon. Weather Rev., 104,* 63, 1976.

Angell, J. K., and J. Korshover, Global ozone variations: An update into 1976, *Mon. Weather Rev., 106,* 725, 1978*a*.

Angell, J. K., and J. Korshover, Recent rocket sonde–derived temperature variations in the western hemisphere, *J. Atmos. Sci., 35,* 1958, 1978*b*.

Arvesen, J. C., R. N. Griffin, and B. D. Pearson, Jr., Determination of extraterrestrial solar spectral irradiance from a research aircraft, *Appl. Opt., 8,* 2215, 1969.

Baulch, D. L., D. D. Drysdale, D. G. Horne, and A. C. Lloyd, *Evaluated Kinetic Data for High Temperature Reactions,* vol. 1, *Homogeneous Gas Phase Reactions of the H_2-O_2 System,* Butterworths, London, 1972.

Baulch, D. L., D. D. Drysdale, D. G. Horne, and A. C. Lloyd, *Evaluated Kinetic Data for High Temperature Reactions,* vol. 2, *Homogeneous Gas Phase Reactions of the H_2-N_2-O_2 System,* Butterworths, London, 1973.

Becker, K. H., W. Groth, and D. Kley, The rate constant of the aeronomic reaction N + O_2, *Z. Naturforsch. A, 24,* 1280, 1969.

Brasseur, G., L'action des oxydes d'azote sur l'ozone dans la stratosphère, *Aeronom. Acta A, 173,* 1–349, 1976.

Brasseur, G., Les Modèles aéronomiques de la stratosphère, *Meteorologie, Vle Sér., 15,* 99, 1978*a*.

Brasseur, G., Un modèle bi-dimensionnel du comportement de l'ozone dans la stratosphère, *Planet. Space Sci., 26,* 139, 1978*b*.

Brasseur, G., On eddy diffusion coefficients, in *Proceedings of the NATO Advanced Study Institute on Atmospheric Ozone, Rep. FAA-EE-80-20,* edited by A. C. Aikin, p. 767, Federal Aviation Administration, Washington, D. C., 1980.

Brasseur, G., and M. Bertin, A theoretical two-dimensional model for minor constituents below 50 km, in *Second International Conference on the Environmental Impact of Aerospace Operations in the High Atmosphere,* American Meteorological Society, Boston, Mass., 1974.

Brasseur, G., and M. Bertin, Distribution and circulation of stratospheric ozone in the meridional plane as given by a two-dimensional model, in *Proceedings of the Joint Symposium on Atmospheric Ozone,* National komitee für Geodäsie und Geophysik bei der Akademie der Wissenschaften der Deutschen Demokratischen Republik, Berlin, 1977.

Brasseur, G., and M. Bertin, The action of chlorine on the ozone layer as given by a zonally averaged two-dimensional model, *Pure Appl. Geophys., 117,* 436, 1978.

Brasseur, G., and M. Nicolet, Chemospheric processes of nitric oxide in the mesosphere and stratosphere, *Planet. Space Sci., 21,* 939, 1973.

Broadfoot, A. L., The solar spectrum 2100–3200 A, *Astrophys. J., 173,* 681, 1972.

Brueckner, G. E., J. D. Bartoe, O. Kjedseth Moe, and M. E. Van Hoosier, Absolute solar ultraviolet intensities and their variations with solar activity, the wavelength region 1750–2100 A, *Astrophys. J., 209,* 935, 1976.

Burrows, J. P., G. W. Harris, and B. A. Thrush, Rates of reaction of HO_2 with HO and O studied by laser magnetic resonance, *Nature, 267,* 233, 1977.

Callis, L. B., and J. E. Nealy, The effect of U.V. variability on stratospheric thermal structure and trace constituents, *Space Res., XVIII,* 95, 1978*a*.

Callis, L. B., and J. E. Nealy, Solar UV variability and its effect on stratospheric thermal structure and trace constituents, *Geophys. Res. Lett., 5,* 249, 1978*b*.

Callis, L. B., M. Natarajan, and J. E. Nealy, Ozone and temperature trends associated with the 11-year solar cycle, *Science, 204,* 1303, 1979.

Clyne, M. A. A., and I. S. McDermid, Mass spectrometric determinations of the rate elementry reactions of NO and NO_2 with ground state N^4S atoms, *J. Chem. Soc. Faraday Trans. 1, 71,* 2189, 1975.

Clyne, M. A. A., and P. B. Monkhouse, Atomic resonance fluorescence for rate constants of rapid bimolecular reactions, H + NO_2 and H + O_3, *J. Chem. Soc. Faraday Trans. 2, 73,* 198, 1977.

Cunnold, D., F. Alyea, N. Phillips, and R. Prinn, A three-dimensional dynamical-chemical model of atmospheric ozone, *J. Atmos. Sci., 32,* 170, 1975.

Cvetanovic, R. J., Excited state chemistry in the stratosphere, *Can. J. Chem., 52,* 1452, 1974.

Davidson, J. A., H. I. Schiff, G. E. Streit, J. R. McAfee, A. L. Schmeltekopf, and C. J. Howard, Temperature dependence of $O(^1D)$ rate constants for reactions with N_2O, H_2, CH_4, HCl and NH_3, *J. Chem. Phys., 67,* 5021, 1977.

Davis, D. D., S. Fischer, and R. Schiff, Flash photolysis-resonance fluorescence kinetics study: Temperature dependence of the reaction OH + CO → CO_2 + H and OH + CH_4 → H_2O + CH_3, *J. Chem. Phys., 61,* 2213, 1973*a*.

Davis, D. D., J. T. Herron, and R. H. Huie, Absolute rate constants for the reaction $O(^3P)$ + NO_2 → NO + O_2 over the temperature range 230°–339°K, *J. Chem. Phys., 58,* 530, 1973*b*.

Delaboudinière, J. P., R. F. Donnelly, H. E. Hinteregger, G. Schmidtke, and P. C. Simon, Intercomparison/compilation of relevant solar flux data related to aeronomy, *Manual 7, COSPAR Tech. Manual Ser.,* Institut d'Aéronomie Spatiale de Belgique, Brussels, 1978.

Demazure, M., and J. Saissac, Généralisation de l'équation classique de diffusion, *Note 115,* l'Etab. d'Etudes et de Rech. Météorol., Paris, 1962.

Demerjian, K. L., J. A. Kerr, and J. C. Calvert, The mechanism of

photochemical smog formation, *Adv. Environ. Sci. Technol., 4,* 1, 1974.

Dickinson, R. E., Method of parametrization for infrared cooling between altitudes of 30 and 70 km, *J. Geophys. Res., 78,* 4451, 1973.

Dubinsky, R. N., and D. J. McKenney, Determination of the rate constant of the $O + H_2 \rightarrow OH + H$ reaction using atomic oxygen resonance fluorescence and the air afterglow techniques, *Can. J. Chem., 53,* 3531, 1975.

Frederick, J. E., Chemical response of the middle atmosphere to changes in the ultraviolet solar flux, *Planet. Space Sci., 25,* 1, 1977.

Gudiksen, P. H., A. W. Fairhall, and R. J. Reed, Roles of mean meridional circulation and eddy diffusion in the transport of trace substances in the lower stratosphere, *J. Geophys. Res.,* 73, 4461, 1968.

Hamilton, E. J., and R. R. Lll, The dependence on H_2O and on NH_3 of the kinetics of the self reaction of HO_2 in the gas-phase formation of $HO_2 \cdot H_2O$ and $HO_2 \cdot NH_3$ complexes, *Int. J. Chem. Kinet., 9,* 875, 1977.

Hampson, R. F., Survey of photochemical and rate data for twenty-eight reactions of interest in atmospheric chemistry, *J. Phys. Chem., 2,* 267, 1973.

Hampson, R. F., and D. Garvin, Reaction rate and photochemical data for atmospheric chemistry—1977, *NBS Spec. Publ. U.S., 513,* 1978.

Heath, D. F., Space observations of the variability of solar irradiance in the near and far ultraviolet, *J. Geophys. Res., 78,* 2779, 1973.

Heath, D. F., Spatial and temporal variability of ozone as seen from space, in *Proceedings of the NATO Advanced Study Institute on Atmospheric Ozone, Rep. FAA-EE-80-20,* edited by A. C. Aikin, p. 45, Federal Aviation Administration, Washington, D. C., 1980.

Heath, D. F., and M. P. Thekaekara, The solar spectrum between 1200 and 3000 Å, in *The Solar Output and Its Variation,* edited by O. R. White, p. 193, Colorado Associated Universities Press, Boulder, 1977.

Heroux, L., and H. E. Hinteregger, Aeronomical reference spectrum for solar UV below 2000 Å, *J. Geophys. Res., 83,* 5305, 1978.

Heroux, L., and R. A. Swirbalus, Full-disk solar fluxes between 1230 and 1940 Å, *J. Geophys. Res., 81,* 436, 1976.

Hinteregger, H. E., Representations of solar EUV fluxes for aeronomical applications, *Space Res., XXI,* in press, 1980.

Hinteregger, H. E., D. E. Bedo, and J. E. Manson, EUV flux variations with solar rotation observed during 1974–1976 from AE-C satellite, *XVII,* 533, 1977.

Howard, C. J., Recent developments in atmospheric HO_2 chemistry, in *WMO Symposium on the Geophysical Aspects and Consequences of Changes in the Composition of the Stratosphere,* World Meteorological Organization, Geneva, 1978.

Humphreys, W. J., Solar disturbances and terrestrial temperatures, *Astrophys. J., 32*(2), 97, 1910.

Kjeldseth Moe, O., M. E. Van Hoosier, J. D. F. Bartoe, and G. E. Brueckner, A spectral atlas of the sun between 1175 and 2100 Å, *Rep. 8056,* Nav. Res. Lab., Washington, D. C., 1976.

Kostkowski, H. J., Spectral irradiance scale change, *Opt. Rad. News NBS, 3,* 5, 1974.

Leu, M. T., and W. B. DeMore, Rate constants at 295 K for the reactions of atomic chlorine with H_2O_2, HO_2, O_3, CH_4 and HNO_3, *Chem. Phys. Lett., 41,* 121, 1976.

Lloyd, A. C., Evaluated and estimated kinetic data for phase reactions of the hydroperoxyl radical, *Int. J. Chem. Kinet., 6,* 169, 1974.

London, J., and S. Oltmans, Further studies of ozone and sunspot, *Pure Appl. Geophys., 106–108,* 1302, 1973.

Luther, F. M., Monthly mean values of eddy diffusion coefficients in the lower stratosphere, paper presented at the AIAA/AMS International Conference on the Environmental Impact of Aerospace Operations in the High Atmosphere, Am. Inst. of Aeronaut. and Astronaut./Am. Meteorol. Soc., Denver, Colo., 1973.

Margitan, J. J., F. Kaufman, and J. G. Anderson, Kinetics of the reaction $OH + HNO_3 \rightarrow H_2O + NO_3$, *Int. J. Chem. Kinet., Symp. 1,* 281, 1975.

Mount, G. N., G. J. Rottman, and J. G. Timothy, The solar spectral irradiance 1200–2250 Å at solar maximum, *J. Geophys. Res., 85,* 4271, 1980.

National Aeronautics and Space Administration, Chlorofluoromethanes and the stratosphere, *NASA Ref. Publ. 1010,* Washington, D. C., 1977.

National Aeronautics and Space Administration, The stratosphere: Present and future, *NASA Ref. Publ. 1044,* Washington, D. C., 1979.

Neckel, H., and D. Labs, Improved data of solar spectral irradiance from 0.33 to 1.25 μm, *Solar Phys.,* in press, 1981.

Nicolet, M., Aeronomic reactions of hydrogen and ozone, in *Mesospheric Models and Related Experiments,* edited by G. Fiocco, p. 1, D. Reidel, Hingham, Mass., 1971.

Nicolet, M., On the production of nitric oxide by cosmic rays in the mesosphere and stratosphere, *Planet. Space Sci., 23,* 637, 1975*a*.

Nicolet, M., Stratospheric ozone: An introduction to its study, *Rev. Geophys. Space Phys., 13,* 593, 1975*b*.

Nicolet, M., and W. Peetermans, The production of nitric oxide in the stratosphere by oxidation of nitrous oxide, *Ann. Geophys., 28,* 751, 1972.

Paetzold, H. K., The influence of solar activity on the stratospheric ozone layer, *Pure Appl. Geophys., 106–108,* 1308, 1973.

Peaceman, D. W., and H. H. Rachford, Jr., The numerical solution of parabolic and elliptic differential equations, *J. Soc. Indust. Appl. Math., 3,* 28, 1955.

Penner, J. E., and J. S. Chang, Possible variations in atmospheric ozone related to the eleven-year solar cycle, *Geophys. Res. Lett., 5,* 817, 1978.

Penner, J. E., and J. S. Chang, The relation between atmospheric trace species variabilities and solar UV variability, *J. Geophys. Res.,* in press, 1980.

Penner, J. E., and F. M. Luther, Effect of temperature feedback and hydrostatic adjustment in a stratospheric model, *J. Atmos. Sci.,* in press, 1980.

Pollack, J. B., W. J. Borucki, and O. B. Toon, Are solar spectral variations a drive for climatic change?, *Nature, 282,* 606, 1979.

Quiroz, R. S., Stratospheric temperatures during solar cycle 20, *J. Geophys. Res., 84,* 2415, 1979.

Reed, R. J., and K. E. German, A contribution to the problem of stratospheric diffusion by large-scale mixing, *Mon. Weather Rev., 93,* 313, 1965.

Rottman, G. J., Rocket measurements of solar spectral irradiance during solar minimum, 1972 to 1977, *J. Geophys. Res.,* in press, 1981.

Ruderman, M. A., and J. W. Chamberlain, Origin of the sunspot modulation of ozone: Its implications for stratospheric NO injection, *Planet. Space Sci., 23,* 247, 1975.

Rycroft, N. J., and A. G. Theobald, Estimates of the stratospheric temperature variation in response to changes of the flux of solar UV radiation, *Space Res., XVIII,* 99, 1978.

Samain, D., and P. C. Simon, Solar flux determination in the spectral range 150–210 nm, *Solar Phys., 49,* 33, 1976.

Schmidtke, G., Todays knowledge of the solar EUV output and the future needs for more accurate measurements for aeronomy, *Planet. Space Sci., 26,* 347, 1978.

Simon, P. C., Balloon measurements of solar fluxes between 1960 Å and 2300 Å, in *Proceedings of the Third Conference on the Climatic Impact Assessment Program, DOT-TSC-OST-74-15,* edited by T. Broderick and T. Hard, p. 137, U. S. Department of Transportation, Washington, D. C., 1974.

Simon, P. C., Nouvelles mesures de l'ultraviolet solaire dans la stratosphère, *Bull. Cl. Sci. Acad. R. Belg., 61,* 399, 1975.

Simon, P. C., Irradiation solar flux measurements between 120 and 400 nm: Current position and future needs, *Planet. Space Sci., 26,* 355, 1978.

Simon, P. C., Observation of the solar ultraviolet radiation, in *Proceedings of the NATO Advanced Study Institute on Atmospheric Ozone, Rep. FAA-EE-80-20,* edited by A. C. Aikin, p. 529, Federal Aviation Administration, Washington, D. C., 1980.

Simon, P. C., R. Pastiels, and D. Nevejans, Balloon observations of solar ultraviolet irradiance at solar minimum, *Planet. Space Sci.,* in press, 1981.

Simon, P. C., Solar irradiance between 120 and 400 nm and its variations, *Solar Phys.,* in press, 1981.

Trenberth, K. E., Global model of the general circulation of the atmosphere below 75 kilometers with an annual heating cycle, *Mon. Weather Rev., 101,* 287, 1973.

Vidal-Madjar, A., Evolution of the solar Lyman alpha flux during four consecutive years, *Solar Phys., 40,* 69, 1975.

Warneck, P., Cosmic radiation as a source of odd nitrogen in the stratosphere, *J. Geophys. Res., 77,* 6589, 1972.

Watson, R. T., Rate constants for reactions of ClO_x of atmospheric

interest, *J. Phys. Chem. Ref. Data, 6,* 871, 1977.
Willett, H. C., The relationship of total atmospheric ozone to the sunspot cycle, *J. Geophys. Res., 67,* 661, 1962.
Wilson, W. E., Jr., A critical review of the gas-phase reaction kinetics of the hydroxyl radical, *J. Phys. Chem. Ref. Data, 1,* 535, 1972.
Wong, W., and D. D. Davis, A flash photolysis-resonance fluorescence study of the reaction of atomic hydrogen with molecular oxygen: $H + O_2 + M \rightarrow HO_2 + M$, *Int. J. Chem. Kinet., 6,* 401, 1974.
Zahniser, M. S., and C. J. Howard, Paper title, in *WMO Symposium on the Geophysical Aspects and Consequences of Changes in the Composition of the Stratosphere,* World Meteorological Organization, Geneva, 1978.
Zahniser, M. S., J. S. Chang, and F. Kaufman, Chlorine nitrate: Kinetics of formation by $ClO + NO_2 + M$ and of reaction with OH, *J. Chem. Phys., 67,* 997, 1977.

(Received January 30, 1980;
revised December 1, 1980;
accepted December 15, 1980.)